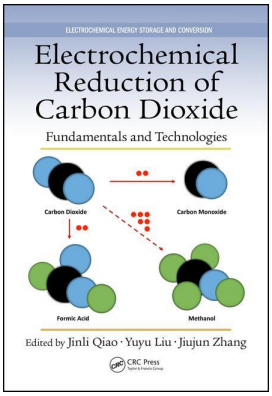

Electrochemical Reduction of Carbon Dioxide Fundamentals and Technologies

Jinli Qiao, Yuyu Liu, Jiujun Zhang

Electrode Kinetics of CO Electroreduction

Publication details
https://test.routledgehandbooks.com/doi/10.1201/b20177-4
Jinli Qiao, Yuyu Liu, Jiujun Zhang
Published online on: 14 Jun 2016

3 Electrode Kinetics of CO_2 Electroreduction

Dongmei Sun and Yu Chen

CONTENTS

3.1 Introduction 103
3.2 Electrochemical Kinetics 107
3.2.1 Certain Aspects of Electrochemical Kinetics 107
3.2.2 Overpotentials 111
3.2.2.1 Basic Concept 111
3.2.2.2 Butler–Volmer Equation 114
3.2.2.3 Overpotential of CO_2 Electroreduction 115
3.3 Mass Transfer near the Electrode Surface 119
3.3.1 Fick's Laws 119
3.3.2 Solubility of CO_2 121
3.3.3 Influences of CO_2 Mass Transfer Near the Electrode Surface 121
3.4 Kinetics and Catalysis of CO_2 Electroreduction 124
3.4.1 Steps in CO_2 Electroreduction 124
3.4.2 Dynamic Influences on CO_2 Electroreduction 125
3.4.3 Turnover Frequency of CO_2 Hydrogenation 125
3.4.4 Reaction Kinetics and Mechanism of CO_2 Electroreduction 126
3.4.4.1 Metal Electrodes 126
3.4.4.2 Molecular Electrocatalysts 130
3.4.4.3 Electrocatalytic Activity Degradation 139
3.5 Product Distribution and Competitive Reduction between CO_2 and Solvent 139
3.5.1 Product Distribution 139
3.5.2 Competitive Reduction between CO_2 and Solvent 140
3.6 Summary and Challenges 144
References 146

3.1 INTRODUCTION

Electrochemical reduction of carbon dioxide (ERC) is an attractive way to convert CO_2 because of the following advantages over thermochemical methods: (1) water is the proton source; (2) high equilibrium conversion at ambient temperature; and (3) relatively simple and green [1].

The electrochemical reduction of CO_2 has been studied since the late nineteenth century [2]. In 1904 [3], Coehn and Jahn used zinc, amalgamated zinc, and

amalgamated copper with high hydrogen overpotential as cathodes to electrolytically reduce carbon dioxide in aqueous $NaHCO_3$ and K_2SO_4 solutions, in which formic acid was the only product.

Most of the reduction reaction of CO_2 occurs in the potential range in which hydrogen evolution reaction (HER) due to hydrolysis of water occurs [4], as the overall standard redox potentials for ERC are in the same range as that for the reduction of protons to H_2. For example [5,6],

	E^0, V (SHE)@298 K (pH = 14)	
Cathode: $CO_2(aq) + H_2O + 2e^- \rightarrow HCOO^- + OH^-$	−1.02	(3.1)
$2H_2O + 2e^- \rightarrow H_2 + 2OH^-$	−0.83	(3.2)

Reaction (3.1) is considered a kinetically "slow" process, occurring at cathode potentials from about −0.8 to −1.8 V vs. a standard hydrogen electrode (SHE) depending on the CO_2 pressure, current density, and catholyte pH, with overpotential ranging from about −0.4 to −1.4 V. The intrinsic kinetics of Reaction (3.1) is said to be independent of pH ($2 < pH < 8$), but a pH above 6 can have a strong effect on the mass transfer limiting current for this reaction, as $CO_2(aq)$ is depleted through the $CO_2(aq)/HCO_3^-/CO_3^{2-}$ equilibria. Reaction (3.2) is thermodynamically favored over Reaction (3.1) over almost the entire pH range at 298 K. However, Reaction (3.1) is kinetically favored over Reaction (3.2) on a group of "high hydrogen overpotential" cathodes, which leads to the high selectivity of formate/formic acid observed by many researchers. The most studied of this favored group of cathode materials are Hg, In, Pb, and Sn, but it is not clear which of these metals is the best because their performance seems to depend on other variables such as CO_2 pressure, catholyte composition, potential, and temperature.

As discussed, increase in the reduction rate of carbon dioxide may also lead to the reduction of water, which will result in hydrogen formation, lowering current efficiency (CE) in ERC. To compete with alternative processes successfully, carbon dioxide reduction must take place at low potential with high efficiency and selectivity at high current densities. The key to this process is to find a stable catalyst with high overpotential for hydrogen evolution and affinity for CO_2, allowing further H^+ transfer steps selectively toward forming methanol. Alternative ways of suppressing HER include operating at high CO_2 pressure and to use solid polymer electrolyte membrane reactor to increase the availability of CO_2 at the electrocatalyst. Copper, both metallic and in oxides form, is considered a promising electrode material as it offers intermediate hydrogen overvoltage and produces more reduced form of carbon dioxide, such as methanol, ethane, methane, and ethylene. As the potential becomes more negative, the generated carbon monoxide/formate suppresses hydrogen evolution.

Many efforts have been made to fundamental studies of the mechanisms and kinetics of ERC on a variety of electrode surfaces [5,7–9]. The reaction pathways and resulting product distributions can be very complex, because they are not only related to the energies of adsorption of a whole range of possible species, including

reactants, intermediates, and products, but also depend on the electrocatalyst property, proton availability, identity of electrolyte and applied cathode potential, carbon dioxide concentration, mass transport, pH, and temperature.

The lowest unoccupied molecular orbital (LUMO) of CO_2 is found predominantly on the carbon atom and most of proposed electrocatalytic reduction mechanisms proceed via high-energy intermediate of $\cdot CO_2^-$ as shown in Figure 3.1 [10]. The transition between CO_2(ads) and $\cdot CO_2^-$(ads) has been suggested to be a common critical limiting step seen by the elbow in plots of j against overpotential common to most systems regardless of the end product produced [11]. This high-energy intermediate is associated with the changing geometry of the linear CO_2 molecule to the bent $\cdot CO_2^-$ radical ion, resulting in the observed high overpotential for CO_2 reduction [12]. The detailed mechanistic pathways for each product are not clear at present, and in many cases several different schemes have been proposed. For example, Figure 3.1 shows the most commonly proposed pathways for ERC at Cu electrode in aqueous solution to carbon monoxide, formic acid, methane, ethylene, and ethane [10,11,13–15].

Step A, the adsorption of CO_2 onto the electrode surface was suggested [8,16,17] prior to CO_2 reduction. Sometimes, an intermediate hydration step (step A_1') is required before the adsorption (step A_2') occurs. In this case, the low solubility of CO_2 in water, that is, 0.070 M at STP conditions, will limit the availability of CO_2(aq) and thus limit the CO_2(ad) concentration on the cathode surface, especially when CO_2 reacts competitively to give HCO_3^- / CO_3^{2-} in alkaline solution. The use of gas phase flow should overcome this limitation by allowing the formation of CO_2(ad) directly from the gaseous state (step A) [11], and catalysts that have high affinity to CO_2 or low activation energy for adsorbing CO_2 should help raise the concentration of CO_2(ad). In addition, ways of increasing CO_2 solubility can be useful in aqueous

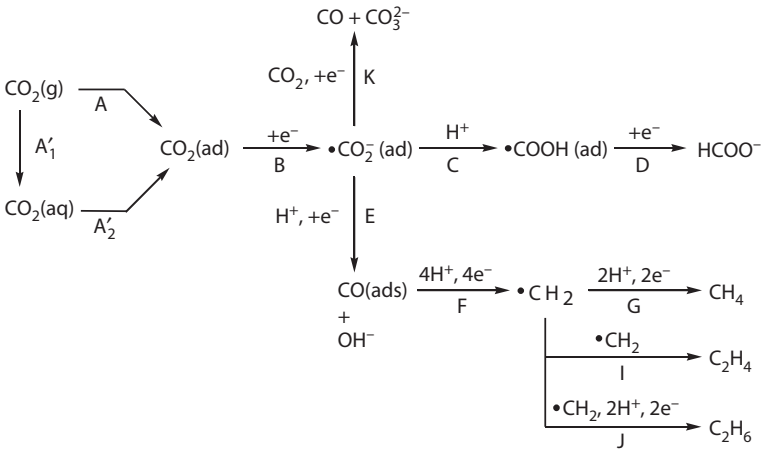

FIGURE 3.1 Mechanistic pathways commonly proposed for ERC at Cu electrode. (Reproduced from the *Electrochimica Acta*, 10, Kaneco, S. et al. Electrochemical reduction of carbon dioxide to ethylene with high Faradaic efficiency at a Cu electrode in CsOH/methanol, 4701–4706, Copyright 1999, with permission from Elsevier.)

systems, such as operating under high pressure or low temperature and using additives to enhance the solubility of CO_2.

Step B is the one-electron reduction of CO_2(ads) to the intermediate radical $\cdot CO_2^-$ species, whose standard redox potential is about –1.9 V [18,19] or –1.85 V [20] vs. SHE in aqueous media, –2.21 V vs. saturated calomel electrode (SCE) in dimethylformamide (DMF) [21].

Adsorbed ·COOH species formed by the protonation reaction in carboxylic form, unless stabilized, will tend to revert back to M–H+CO_2 or undergo nucleophilic attack to give M–CO^+ (i.e., M–C=O). This reactive intermediate is thought to be commonly formed for Cu, Ru, and some other d-block metals and is believed to be present in the pathways resulting in highly reduced products.

Step E is the second electronation/protonation to produce a key intermediate species of adsorbed CO for the formation of an adsorbed reactive methylene group, which could be stabilized as CH_4, be dimerized to C_2H_4 or be transformed to C_2H_6.

Pacansky et al. studied self-consistent field (SCF) ab initio molecular orbital energies and atomic population analysis of $\cdot CO_2^-$ at the minimum energy geometry (Figure 3.2). According to their analysis, the unpaired electron density at the highest occupied orbital is localized at C atom at 84% [22]. This result suggests that $\cdot CO_2^-$ is ready to react as a nucleophilic reactant at the carbon atom. Along this line, the weakly adsorbed $\cdot CO_2^-$ goes through a protonation reaction, then there is a second electron transfer to yield formate (steps B–C–D). A parallel disproportionation of the adsorbed $\cdot CO_2^-$ radical anion produces CO (steps B–K) [11,14,23].

It is seen from Table 3.1 that the overall standard redox potentials for ERC are in the same range as that for the reduction of protons to H_2 ($E^0 = 0.0$ V [SHE]), which indicates that ERC is not thermodynamically much more difficult than hydrogen evolution. However, ERC is kinetically suppressed because of the high-energy intermediate radical $\cdot CO_2^-$ and the involvement of multielectron transfer, that is, 2 electrons for $HCOO^-$ (steps B–C–D) and 8 electrons for CH_4 (steps B–E–F–G).

Research on ERC is still at a stage of fundamental investigations on mechanisms and kinetics using tiny electrodes (e.g., 1×10^{-4} m^2) with little consideration of the possibility for practical application. Research on the engineering aspects of ERC should be initiated to bridge the gap between the previous laboratory work and industrial reality. Such engineering research includes the design and scale-up of continuous electrochemical reactors, together with the conception, design, and economic projections for complete ERC processes. Akahori et al., who are apparently the first to report continuous operation, used a lead wire bundle cathode in a flow-by reactor with a cation membrane separator. This reactor obtained a formate CE near 100%

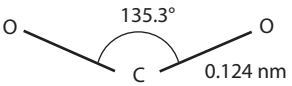

FIGURE 3.2 Atomic configuration of $\cdot CO_2^-$. (Reproduced with permission from Pacansky, J., Wahlgren, U. and Bagus, P. S. SCF ab-initio ground state energy surfaces for CO_2 and CO_2^-. *The Journal of Chemical Physics.* 62(7): 2740–2744. Copyright 1975, American Institute of Physics.)

TABLE 3.1
Standard Potential for CO_2 Electroreduction Reactions in Aqueous Media at 25°C

Reaction	E^0/V vs. SHE	$E^{0'}$/V vs. SHE[b]
$CO_2 + e^- = \cdot CO_2^-$	−1.90	–
$CO_2 + 2H^+ + 2e^- = CO + H_2O$	−0.10	−0.52
$CO_2 + 2H^+ + 2e^- = HCOOH$	−0.20	−0.61
$2CO_2 + 2H^+ + 2e^- = H_2C_2O_4$	−0.475	−0.889
$CO_2 + 4H^+ + 4e^- = HCHO + H_2O$	−0.071	−0.485
$CO_2 + 6H^+ + 6e^- = CH_3OH + H_2O$	0.03	−0.38
$CO_2 + 8H^+ + 8e^- = CH_4 + 2H_2O$	0.17	−0.24
$2CO_2 + 12H^+ + 12e^- = C_2H_4 + 4H_2O$	0.07	−0.34
$2CO_2 + 12H^+ + 12e^- = C_2H_5OH + 3H_2O$	0.085	−0.3287
$3CO_2 + 18H^+ + 18e^- = C_3H_7OH + 5H_2O$	0.09	−0.3237
$2H^+ + 2e^- = H_2$	0	−0.414

Source: Reproduced from Chaplin, R. P. S. and Wragg, A. A. *Journal of Applied Electrochemistry*. 2003; 33(12): 1107–1123. With permission of Kluwer.

with single-phase flow of a CO_2-saturated catholyte solution at 1.4 mL min^{-1} and current about 2 mA (0.02 kA m^{-2}). Li and Oloman [24] described the electroreduction of CO_2 in a laboratory bench-scale continuous reactor using a flow-by three-dimensional (3D) cathode of 30# mesh tinned copper, with the variables: current (1–8 A), gas phase CO_2 concentration (16–100 vol%), and operating time (10–180 min), in operation near ambient conditions (ca. 115 kPa [abs], 300 K). For superficial current densities ranging from 0.22 to 1.78 kA m^{-2}, the measured CE, which is one of the performance indicators for electrochemical processes, for $HCOO^-$ = 86%–13%, reactor voltage = 3–6 V, specific energy for $HCOO^-$ = 300–1300 kWh $kmol^{-1}$, space-time yield of $HCOO^- = 2 \times 10^{-4}$–$6 \times 10^{-4}$ kmol m^{-3} s^{-1}, conversion of CO_2 = 20%–80%, and yield of organic products from CO_2 = 6%–17%. The initial electroactive species in a primary reaction is subjected to CO_2 mass transfer constraint, with CE depending on the current density and partial pressure of CO_2 in the gas phase, together with the hydrogen overpotential and mass transfer capacity of the 3D cathode. Figure 3.3 shows the process flow diagram.

3.2 ELECTROCHEMICAL KINETICS

3.2.1 Certain Aspects of Electrochemical Kinetics

The electrochemical reaction occurs at the interface between the electrode (an electronic conductor) and electrolyte solution (an ionic conductor), composed of a series of steps always includes these three steps: (1) the approach of the reactant species to the electrode surface (first mass transfer); (2) the reaction via heterogeneous electron

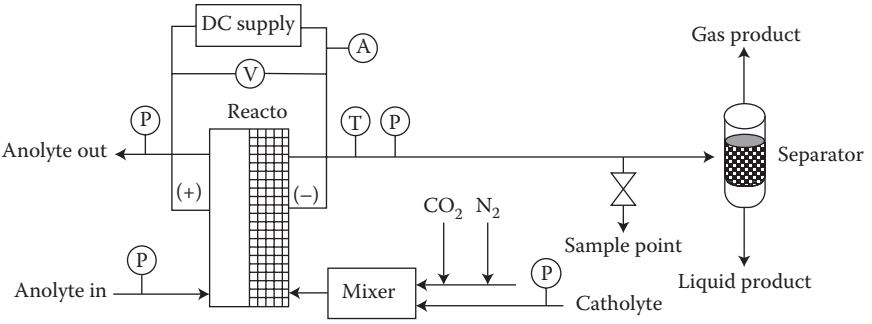

FIGURE 3.3 Process flow diagram. A = ammeter, p = pressure gauge, T = thermometer, V = voltmeter. (With kind permission from Springer Science+Business Media: *Journal of Applied Electrochemistry*, The electro-reduction of carbon dioxide in a continuous reactor, 35(10), 2005, 955–965, Li, H. and Oloman, C.)

transfer across the interface (actual electrochemical step); and (3) the movement of the product species away from the reaction area into bulk solution (second mass transfer). The actual electrochemical step can be accompanied by different chemical reactions, either in bulk or on the electrode surface. Some of these processes, such as electron transfer at the electrode surface or adsorption, depend upon the electrode potential. Determination of a possible step order and the rate-determining step (r.d.s.) is crucial for the dynamic description of a specific electrode process [25].

For a given electrode reaction:

$$\mathrm{O} + \mathrm{ne} \underset{k_b}{\overset{k_f}{\rightleftharpoons}} \mathrm{R} \tag{3.3}$$

where both oxidized form, O, and reduced form, R, of a redox couple are initially present in the bulk solution.

The rate of the forward reduction process, v_f, is

$$v_f = k_f C_O(0,t) = \frac{i_c}{nFA} \tag{3.4}$$

whereas the rate of the backward oxidation reaction, v_b, is

$$v_b = k_b C_R(0,t) = \frac{i_a}{nFA} \tag{3.5}$$

where k_f/k_b is the forward/backward rate constant, $C_O(0, t)/C_R(0, t)$ is the surface concentration of O/R at time t, and i_c/i_a is the cathodic/anodic current. The net reaction rate is

$$v_{net} = v_f - v_b = k_f C_O(0,t) - k_b C_R(0,t) = \frac{i}{nFA} \tag{3.6}$$

in which the overall current is

$$i = i_c - i_a = nFA[k_f C_O(0,t) - k_b C_R(0,t)] \tag{3.7}$$

An accurate kinetic picture of an electrode process is often gained by determining current as a function of potential because there is a proportionality between the current and the net rate of an electrode reaction, and the reaction rate is a strong function of the electrode potential. At equilibrium, the net current is zero, and the electrode potential is defined by the Nernst equation:

$$E = E^{0'} + \frac{RT}{nF} \ln \frac{C_O^*}{C_R^*} \tag{3.8}$$

where C_O^*/C_R^* is the bulk concentration of O/R, and $E^{0'}$ is the former potential. Upon passage of Faradaic current, the electrode potential deviates from its equilibrium value and this is termed electrode polarization. The extent of polarization is determined by the overpotential, η,

$$\eta = E - E_{\text{eq}} \tag{3.9}$$

Based on Butler–Volmer's model of electrode kinetics, for a single one-step, one-electron reversible electrode process without any other chemical step

$$O + e \underset{k_b}{\overset{k_f}{\rightleftharpoons}} R \tag{3.10}$$

The derived current–overpotential equation is

$$i = i_0 \left[\frac{C_O(0,t)}{C_O^*} e^{-\alpha f \eta} - \frac{C_R(0,t)}{C_R^*} e^{(1-\alpha) f \eta} \right] \tag{3.11}$$

where $f = F/RT$, α is the transfer coefficient, and i_0 is the exchange current, which represents the balanced Faradaic current at equilibrium and is equal to either component current, i_c or i_a in magnitude. The value of i_0 can be calculated by

$$i_0 = FAk^0 C_O^* e^{-\alpha f (E_{\text{eq}} - E^{0'})} \tag{3.12}$$

The curve in Figure 3.4 shows the behavior of Equation 3.11, from which we can see that for the cathodic branch at high η, the anodic component i_a is insignificant, whereas the anodic contribution i_c is negligible at large positive overpotentials, and the total current is the sum of the components i_c and i_a. At extreme η, the current levels off, reaching a cathodic limiting current, $i_{l,c}$ or an anodic limiting current, $i_{l,a}$,

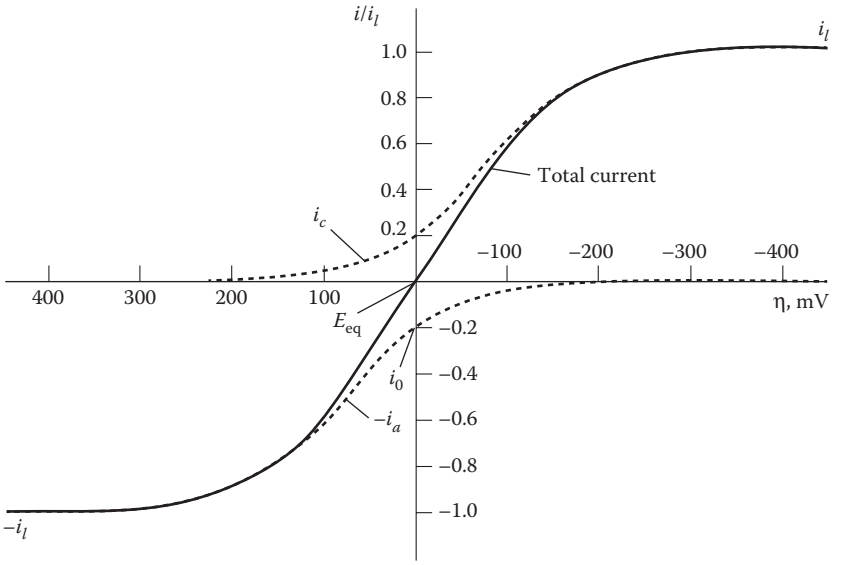

FIGURE 3.4 Current–overpotential curves for the system with $\alpha = 0.5$, $T = 298$ K, $i_{l,c} = -i_{l,a} = i_l$, and $i_0/i_l = 0.2$. The dashed lines show the component currents i_c and i_a. (Bard, A. J. and Faulkner, L. R..: *Electrochemical Methods Fundamentals and Applications*. 2nd ed. p. 100. 2001. Copyright Wiley-VCH Verlag GmbH & Co. KGaA. Reproduced with permission.)

which is limited by mass transfer rather than heterogeneous kinetics and the overpotential is a concentration overpotential. At certain η, the electrode process could have several slow steps and the current is driven by overpotentials associated with different reaction steps: η_{mt} (mass transfer overpotential), η_{ct} (charge-transfer overpotential), and $\eta_{r\times n}$ (the overpotential associated with a preceding reaction).

The actual relationship between the current and the electrode overpotential usually depends on the nature of the limiting step, which allows hypothesizing about the character of the investigated process.

1. No mass transfer effects
   When mass transfer effects are not included, Equation 3.11 becomes

$$i = i_0[e^{-\alpha f\eta} - e^{(1-\alpha)f\eta}] \quad \text{O} + \text{e} \underset{k_b}{\overset{k_f}{\rightleftarrows}} \text{R} \tag{3.13}$$

   known as the Butler–Volmer equation historically. The overpotential here is solely for driving the heterogeneous process at the rate reflected by the current. The lower the exchange current, the larger the activation overpotential for any particular net current, indicating more sluggish kinetics.
2. Linear characteristic at small η
   When the value of η is sufficiently small, Equation 3.11 can be expressed as

$$i = -i_0 f\eta \tag{3.14}$$

which indicates that the corresponding $i - \eta$ curve near E_{eq} in a narrow potential range is linear with negative reciprocal slope of $-\eta/i$, which is often called the charge-transfer resistance, R_{ct}

$$R_{ct} = \frac{RT}{Fi_0} \tag{3.15}$$

serving as a convenient index of kinetic facility.

3. Tafel behavior at large η

At large negative/positive overpotentials, one of the bracketed terms in Equation 3.13 becomes negligible. When $\exp(-\alpha f\eta) \gg \exp[(l - \alpha)f\eta]$ for a cathodic branch, Equation 3.13 becomes

$$i = i_0 e^{-\alpha f \eta} \tag{3.16}$$

or expressed as

$$\eta = \frac{RT}{\alpha F} \ln i_0 - \frac{RT}{\alpha F} \ln i \tag{3.17}$$

Compared with the empirical Tafel equation given by Tafel in 1905

$$\eta = a + b \log i \tag{3.18}$$

the constants can now be identified from theory as [25]

$$a = \frac{2.3RT}{\alpha F} \log i_0, \quad b = \frac{-2.3RT}{\alpha F} \tag{3.19}$$

Tafel behavior is an indicator of totally irreversible kinetics. A plot of log i vs. η, known as a Tafel plot (Figure 3.6), is useful for the evaluation of kinetic parameters, such as α, i_0 when applied, though it sharply deviates from linear behavior when η approaches zero.

3.2.2 Overpotentials

3.2.2.1 Basic Concept

The overpotential is the difference between the applied electrode potential, $E_{applied}$, and E^0 (products/substrates), at a given current density, reflecting the degree of deviation of the electrode potential from its thermodynamic equilibrium value from the Nernst equation. In other words, an overpotential is the extra amount of nonreversible energy required to overcome the energy barrier which allows the reaction to occur. It shows how far away the electrode is from its equilibrium.

The electrode overpotential mainly consists of three components: concentration overpotential, η_{con}; activation overpotential, η_{act}; and ohmic overpotential, η_{ohmic}, expressed as follows:

$$\eta = \eta_{ohmic} + \eta_{con} + \eta_{act} \tag{3.20}$$

where η is the overall overpotential. Other additional overpotentials may exist, such as the chemical reaction overpotential. The cell overpotential cannot be eliminated but can be minimized by proper material modification and good cell design. Furthermore, cell working atmosphere, such as pressure and temperature, can also influence the overpotential.

3.2.2.1.1 Ohmic Losses

The ohmic losses are due to resistance created when ions are moving through the electrolyte and electrons moving through the electrode, including the Pt lead wire resistance, electrode resistance, electrolyte resistance, etc. According to Ohm's law:

$$\eta_{ohmic} = IR \tag{3.21}$$

where R is the ohmic resistance. By knowing the conductivity (κ), conducting length (l), and cross-section area (A_0), the ohmic resistance of such geometry can be calculated by

$$R = \frac{l}{\kappa A_0} \tag{3.22}$$

Equipotential plane is required to estimate the ohmic resistance of a conductor when the above equation is used. The resistance of a lead wire can be easily evaluated by knowing its conductivity. However, the electrolyte and electrode resistances cannot be directly estimated because the electrochemical reactions at the interface of the electrode and electrolyte cause a nonequipotential plane. An average ohmic resistance is sought. For example, a porous Pt electrode can be viewed as numerous cylindrical pores surrounded by Pt blocks. Each Pt block and electrolyte forms a resistor, as illustrated in Figure 3.5.

The average resistance can therefore be calculated as these numerous resistors are aligned in parallel:

$$R = \frac{l}{\kappa(1-\varepsilon)A_0} \tag{3.23}$$

where ε is the electrode porosity, and A_0 is the electrode physical area. Equation 3.23 is based on assuming the potential field of each single resistor does not interfere with each other. From the above equations, the electrode and electrolyte resistances can be estimated and compared with experimental measurement.

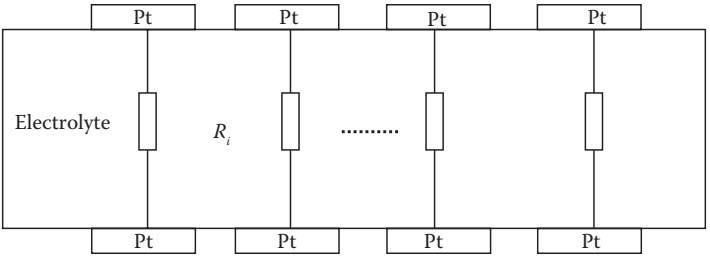

FIGURE 3.5 Illustration of resistors formed by the electrolyte and electrode. (Reproduced from Tao, G. Investigation of carbon dioxide electrolysis reaction kinetics in a solid oxide electrolyzer, 2003. With permission from ProQuest ILC.)

3.2.2.1.2 Concentration Overpotential

A concentration overpotential is caused by the slow diffusion of reactants or products under concentration gradients. It is defined as an external energy required to maintain concentration gradients near the electrode for the sustenance of chemical reactions. This concentration overpotential becomes eminent as mass diffusion effects hinder the entire electrode reaction. For CO_2 electroreduction, mass diffusion includes gas bulk diffusion and adsorbates surface diffusion. When the maximum diffusion rate of transporting species to/from the electrode reaction site is slower than the electrochemical reaction rate, diffusion becomes a r.d.s., and a limiting current is reached.

By Fick's diffusion law [27], the limiting current density can be calculated by assuming the reactant concentration at the reaction site is zero:

$$i_L = \frac{nFDC_B}{\delta} \tag{3.24}$$

where D is the diffusivity, C_B is the reactant bulk concentration, and δ is the thickness of the diffusion layer. Assuming the charge-transfer reaction rate at the electrode is so high that the activation overpotential is negligible compared with the concentration overpotential. The concentration overpotential can therefore be written as

$$\eta_{con} = \frac{RT}{nF} \ln\left(1 - \frac{i}{i_L}\right) \tag{3.25}$$

The concentration overpotential can be reduced by increasing the limiting current, which is a function of concentration and diffusivity as expressed in Equation 3.24. Design of gas bulk diffusion channels and microstructures of an electrode can influence the concentration overpotential.

3.2.2.1.3 Activation Overpotential

Activation overpotential describes an external energy required to overcome the maximum activation energy barrier in order to maintain the electrode reaction at an

appreciable rate. This irreversible potential occurs when the rate of the electrochemical reaction at the electrode is limited by slow electrode kinetics, or charge transfer. It highly depends on the electrode catalytic characteristics.

Activation overpotentials are affected mostly by the oxidation or reduction rate constants. A decrease in the oxidation or reduction rate constant will increase the activation overpotential. The magnitude of the activation overpotential is more than doubled as the redox rate constant decreases by a magnitude of order two. Therefore, one efficient way to improve the CO_2 electroreduction performance is to find a better catalyst with a fast oxidation/reduction rate constant to reduce the activation overpotential. Both the anode and cathode activation overpotentials follow the Tafel behavior, and the charge transfer controls the reaction as discussed below.

3.2.2.2 Butler–Volmer Equation

As discussed in Section 3.2.1, for an electrochemical reaction with multiple steps involving one electron without any other chemical step, the activation overpotential can be correlated to current by the Butler–Volmer equation (3.13).

The transfer coefficients are considered as the fraction of the change in polarization, which leads to a change in the reaction rate constant. The transfer coefficients can be given by the Bockris model as [28]

$$\alpha_a = \frac{n - \gamma_c}{\upsilon} - r\beta \tag{3.26}$$

$$\alpha_c = \frac{\gamma_c}{\upsilon} + r\beta \tag{3.27}$$

where α_a and α_c are the anodic and cathodic transfer coefficients, respectively. γ_c is the number of charges transferred ahead of the r.d.s., υ is the total number of times of repeating the r.d.s. reaction to complete the reaction, r is the number of charges transferred in the r.d.s., and β is the symmetric coefficient (usually 0.5). Apparently, the transfer coefficients have the following relationship:

$$\alpha_a + \alpha_c = \frac{n}{\upsilon} \tag{3.28}$$

The exchange current density is a function of reaction rate constants, the concentration of the anodic and cathodic reactants, etc. It is related to the balanced forward and backward electrode reaction rates at equilibrium. A high exchange current density leads to a fast electrochemical reaction, thus good cell performance is anticipated.

A typical Butler–Volmer equation at large activation overpotential is plotted in Figure 3.6 when the exchange current density is 0.001 mA/cm^2 and the anodic and cathodic transfer coefficients are unity. The plot shows a high linearity, indicating the Tafel behavior. The plot is symmetric due to the same anodic and cathodic transfer coefficients. Otherwise, it should be asymmetric.

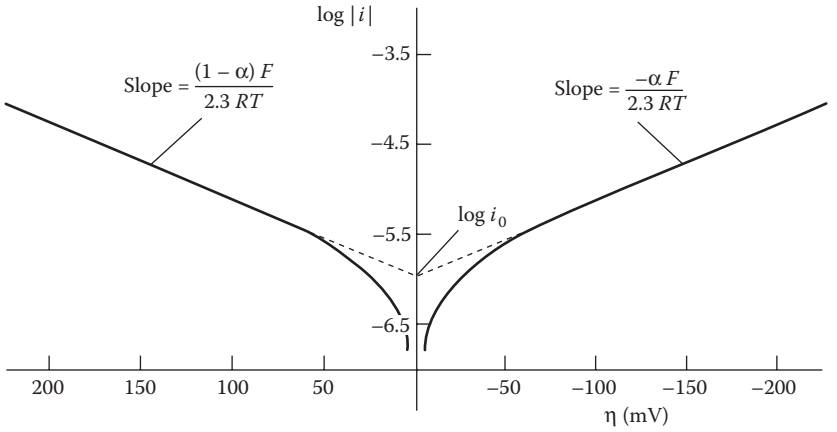

FIGURE 3.6 Tafel plots for anodic and cathodic branches of the current–overpotential curve for $O + e \underset{k_b}{\overset{k_f}{\rightleftharpoons}} R$ with $\alpha = 0.5$, $T = 298$ K, and $j_0 = 10^{-6}$ A/cm^2. (Bard, A. J. and Faulkner, L. R.: *Electrochemical Methods Fundamentals and Applications*. 2nd ed. p. 103. 2001. Copyright Wiley-VCH Verlag GmbH & Co. KGaA. Reproduced with permission.)

3.2.2.3 Overpotential of CO_2 Electroreduction

Direct ERC on most electrode surfaces requires impractically high overpotential which is necessary to drive the process and consequently lowers the conversion efficiency [29].

The standard potential of the reduction of CO_2 to different products as shown in Table 3.1, calculated from the thermodynamic data, is much more positive than that the reduction actually takes place at as shown in Table 3.2. Such high overpotential is presumed from involvement of intermediate species, $\cdot CO_2^-$ anion radical, which requires highly negative potential for the formation. The high overpotential depends on electrode metal, crystal orientation, and reduction product alongside proton availability. CO formation takes place with relatively lower overpotentials than $HCOO^-$ formation. Stabilization of $\cdot CO_2^-$ adsorption on electrodes may lead to reduction of the overpotential. Among all the electrodes, Au electrode reduces CO_2 to CO at remarkably low cathodic potential, –1.14 V at 5 mA cm^{-2} (Table 3.2). It is suggested that the formed intermediate species $\cdot CO_2^-$ on the Au electrode was greatly stabilized by adsorption, leading to decrease of overpotential [30]. Coordination of the CO_2 to M can activate $\cdot CO_2^-$ and promote its reductive disproportionation to form $CO + CO_3^{2-}$.

Clearly, in order to minimize overpotentials, catalysts need to be developed that have formal potentials $E^0(Cat^{n+/0})$ well matched to E^0(products/CO_2), and appreciable rate constants for the electroreduction of CO_2 to appropriate products at this potential. In addition, the heterogeneous rate constant for reduction of the electrocatalyst at the electrode must be high for $V_{applied}$ near $E^0(Cat^{n+/0})$.

Transition metal electrodes have been reported to dramatically reduce the overpotential of reduction to at least 500 mV anodic of E^0 for $CO_2 \rightarrow \cdot CO_2^-$. Bruce et al. [32] find $E^0 = +0.1$ V vs. SHE for $CO_2 + 2H^+ + 2e^- \rightarrow HCOOH$ on copper, which is much more positive than that calculated from Gibbs energy of formation.

TABLE 3.2
Potentials and Faradaic Efficiencies of Products of CO_2 Reduction at Various Metal Electrodes in 0.1 M $KHCO_3$, $T = 18.5 \pm 0.5°C$

			Faradaic Efficiency (%)							
Electrode	Potential vs. SHE V	Current Density (mA cm^{-2})	CH_4	C_2H_4	EtOH[a]	PrOH[b]	CO	$HCOO^-$	H_2	Total
Pb	−1.63	5.0	0.0	0.0	0.0	0.0	0.0	97.4	5.0	102.4
Hg	−1.51	0.5	0.0	0.0	0.0	0.0	0.0	99.5	0.0	99.5
Tl	−1.60	5.0	0.0	0.0	0.0	0.0	0.0	95.1	6.2	101.3
In	−1.55	5.0	0.0	0.0	0.0	0.0	2.1	94.9	3.3	100.3
Sn	−1.48	5.0	0.0	0.0	0.0	0.0	7.1	88.4	4.6	100.1
Cd	−1.63	5.0	1.3	0.0	0.0	0.0	13.9	78.4	9.4	103.0
Au	−1.14	5.0	0.0	0.0	0.0	0.0	87.1	0.7	10.2	98.0
Ag	−1.37	5.0	0.0	0.0	0.0	0.0	81.5	0.8	12.4	94.6
Zn	−1.54	5.0	0.0	0.0	0.0	0.0	79.4	6.1	9.9	95.4
Pd	−1.20	5.0	2.9	0.0	0.0	0.0	28.3	2.8	26.2	60.2
Ga	−1.24	5.0	0.0	0.0	0.0	0.0	23.2	0.0	79.0	102.0
Cu	−1.44	5.0	33.3	25.5	5.7	3.0	1.3	9.4	20.5	103.5[c]
Ni	−1.48	5.0	1.8	0.1	0.0	0.0	0.0	1.4	88.9	92.4[d]
Fe	−0.91	5.0	0.0	0.0	0.0	0.0	0.0	0.0	94.8	94.8
Pt	−1.07	5.0	0.0	0.0	0.0	0.0	0.0	0.1	95.7	95.8
Ti	−1.60	5.0	0.0	0.0	0.0	0.0	not available	0.0	99.7	99.7

Source: Reproduced from *Electrochimica Acta*, 39(11–12), Hori, Y. et al., Electrocatalytic process of CO selectivity in electrochemical reduction of CO_2 at metal electrodes in aqueous media. 1833–1839. Copyright 1994, with permission from Elsevier.

[a] Ethanol.

[b] *n*-propanol.

[c] The total value contains C_3H_5OH (1.4%), CH_3CHO (1.1%), and C_2H_5CHO (2.3%) in addition to the tabulated substances.

[d] The total value contains C_2H_6 (0.2%).

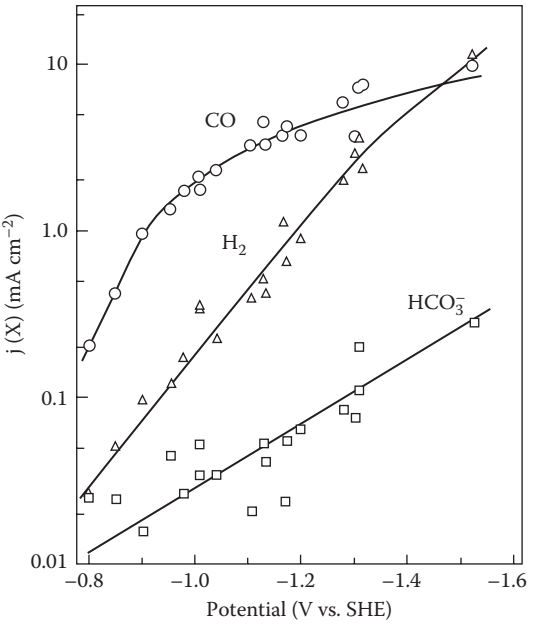

FIGURE 3.7 Partial current densities of the products j(X) vs. electrode potential in CO_2 reduction at an Au electrode. 0.5 M $KHCO_3$, 1 atm CO_2, 18°C. (Hori, Y. et al. Electrochemical reduction of carbon dioxides to carbon monoxide at a gold electrode in aqueous potassium hydrogen carbonate. *Journal of the Chemical Society, Chemical Communications.* 1987; (10): 728–729. Reproduced by permission of the Royal Society of Chemistry.)

Fundamental studies will contribute to enhancement of our understanding of the overpotential of the electrodes. A wide range of Tafel slopes for CO_2 reduction from 120 mV decade^{-1} to 350 mV decade^{-1} has been reported [5,16,33,34]. These slopes indicate a rate-determining initial electron transfer to CO_2 forming a surface adsorbed $\cdot CO_2^-$ intermediate. The calculated exchange current density for the formation of $\cdot CO_2^-$ radical at 100 kPa and 298 K in CO_2-saturated aqueous solution (~0.036 M) is 4.8×10^{-7} kA m^{-2} [35]. The exchange current densities for ERC to formate at 293 K in 0.95 M KCl + 0.05 M $NaHCO_3$ on In, Hg, and Sn are reported, respectively, as 1×10^{-7}, 1×10^{-10}, 1×10^{-8} kA m^{-2} [6].

Gold electrodes yield CO in CO_2 reduction at −0.8 V vs. SHE with a low overpotential in 0.5 M $KHCO_3$ [30]. The obtained relationship between the potential and logarithm of the partial current of CO formation (i_c) (Figure 3.7) showed that the Tafel slope is approximately 130 mV decade^{-1} in the lower current region, where the transport process of CO_2 does not interfere with the supply of CO_2 to the electrode, the Tafel slope corresponds to the transfer coefficient 0.46. i_c at a constant potential is linear to the CO_2 partial pressure. These data suggest that the CO_2 reduction proceeds in the first order with respect to CO_2, and the r.d.s. of the reaction is the first electron transfer to CO_2. These facts support the reaction scheme discussed in the

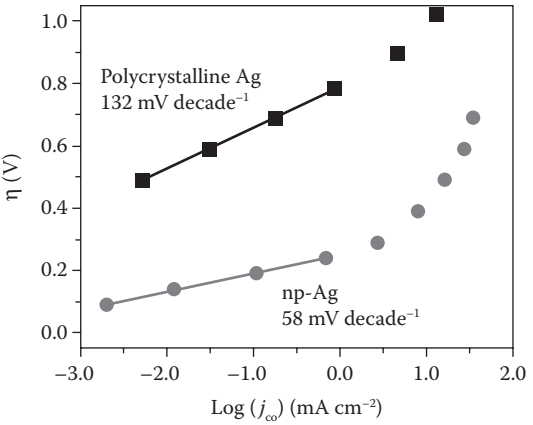

FIGURE 3.8 Overpotential vs. CO production partial current density on polycrystalline silver and np-Ag. (Reproduced by permission from Macmillan Publishers Ltd. *Nature Communications*, Lu, Q. et al. A selective and efficient electrocatalyst for carbon dioxide reduction. 5: 3242, copyright 2014.)

following. In phosphate buffer solutions of pH 2–6.8 at an Au electrode, i_c is proportional to the pressure of CO_2 [36]. The Tafel slope is ca. 120 mV decade^{-1}. The potential partial current relation obtained with electrolytes at pH below 4.3 agreed well with that obtained with 0.5 M $KHCO_3$ at pH 7.5 after the double-layer correction due to the difference of the electrolyte concentration [30]. This fact shows that CO formation at Au electrode does not depend on pH of the electrolyte, and that the proton donor is not H^+ but H_2O molecules.

The intrinsic electrocatalytical activity of nanoporous silver (np-Ag) for CO_2 reduction to CO was investigated through Tafel analysis in a CO_2-saturated 0.5 M $KHCO_3$, compared with polycrystalline Ag catalyst, as shown in Figure 3.8 [37] As observed, the np-Ag was more preferred for CO_2 reduction with a Tafel slope of 58 mV decade^{-1}, much smaller than that of 132 mV decade^{-1} for polycrystalline Ag. At a overpotential higher than 0.25 V, the slope increased sharply, indicating another rate-limiting step most probably relating to the issues of the diffusion of reactants and products out of/into the catalyst nanopores. Mechanistically, there are two steps in the two-electron reduction of CO_2 to CO on an Ag surface [38]. First, one electron is transferred to a CO_2 molecule, forming a $\cdot CO_2^-$ anion intermediate absorbed on the catalyst surface. Subsequently, the CO_2^- anion takes another electron and two protons, forming a molecule of CO and a molecule of H_2O. As reported [39], the first step at a much more negative potential compared with that of the following step is rate determining for the whole process with calculated Tafel slope of 120 mV decade^{-1}. This is very similar to that of 132 mV decade^{-1} observed in polycrystalline Ag. For np-Ag, the sharp decrease of Tafel slope at 58 mV decade^{-1} presents a fast step of initial electron transfer before a r.d.s. of later nonelectron transfer [39–41], indicating that the np-Ag with possibly higher index facets supported by

the highly curved surface [42,43] are able to stabilize the anion $\cdot CO_2^-$ intermediate much better than a flat one.

Results of studies on the kinetics with a copper foil electrode at 273 and 295 K using two separate electrode pretreatments to remove the oxide layer, that is, 10 wt% HCl and 10 wt% HNO_3 [44], is listed in Table 3.3.

The kinetic information/data on ERC is sparse and difficult to summarize because of the variety of approaches and experimental conditions. It has to be noted that the reaction kinetics depend on many interacting factors so results obtained by one researcher under his conditions might not apply under other conditions.

3.3 MASS TRANSFER NEAR THE ELECTRODE SURFACE

3.3.1 Fick's Laws

Diffusion is one of the fundamental processes by which material moves, the macroscopic result of random molecular motion describing the spread of particles, and is an important factor controlling the rate at which many interactions occur. The diffusion coefficient (D) is a parameter indicative of the diffusional mobility of species and encountered most famously in Fick's laws (3.29) and (3.30), but also in numerous other equations throughout physics and chemistry. Fick's first law of diffusion states [45]

$$J = -D\frac{\partial C(x)}{\partial x} \tag{3.29}$$

where J is the diffusion flux, D is the diffusion coefficient, C is concentration, and x is the position in the one-dimensional system. This proportionality of flux of matter to the concentration gradient (3.29) shows that the flux of matter is dependent upon the variation in concentration with position. From this relationship, it is suggested that without a concentration gradient there is no net flux and the diffusive flux would

TABLE 3.3
Kinetic Information of CO_2 Electroreduction to CH_4 on a Cu Foil Cathode at Ambient Pressure

Temperature (K)	Pretreatment	Tafle Slope V/decade	j_o kA m^{-2}	Highest CE %	CE at −1.46 V (SHE) %
273	10 wt% HCl	0.539	N/A	N/A	47
295	10 wt% HCl	0.110	1.94×10^{-7}	50	20
295	10 wt% HNO_3	0.170	N/A	32	N/A

Source: Reproduced from *Journal of Electroanalytical Chemistry and Interfacial Electrochemistry*, 245(1–2), Kim, J. J. et al. Reduction of CO_2 and CO to methane on Cu foil electrodes, 223–244, Copyright 1988, with permission from Elsevier.

Note: Catholyte = 0.5 M $KHCO_3$ at pH = 7.6.

be zero. This first law describes mathematically diffusion within steady-state systems where the concentration is time invariant; however, this is not always the case, which leads to the less specific second law. Fick's second law of diffusion [45]

$$\frac{\partial C(x,t)}{\partial t} = -\frac{\partial J}{\partial x} = D\frac{\partial^2 C}{\partial x^2} \tag{3.30}$$

Fick's second law of diffusion (3.30) predicts the change in concentration (accumulation or depletion) with time as a result of diffusion with t denoting the time. The concentration change is proportional to the diffusion coefficient and the second derivative/curvature of the concentration as illustrated in Figure 3.9. This equation assumes that the diffusion coefficient is independent of composition or the range of compositions is small.

The diffusion coefficient of a species in a given system can be evaluated using the Stokes–Einstein (3.31) and Wilke–Chang (3.32) relations [47,48]:

$$D = \frac{k_B T}{6\pi\eta r} \tag{3.31}$$

$$D = \frac{7.4\times10^{-8}(xM)^{1/2}T}{\eta V^{0.6}} \tag{3.32}$$

In the Stokes–Einstein equation (3.31), k_B is the Boltzmann constant, T is the temperature in K, η is the dynamic viscosity in Pa·s, and r is the molecular radius of the analyte in m to give D in $m^2\ s^{-1}$. In the Wilke–Chang relationship (3.32), x is the association parameter of the solvent, M is the molecular mass of the solvent in u, T is the temperature in K, η is the dynamic viscosity in cP or mPa·s, and V is the molar volume of analyte at boiling point under standard conditions in $cm^3\ mol^{-1}$ to give the diffusion coefficient in $cm^2\ s^{-1}$. Some of the most well utilized electrochemical

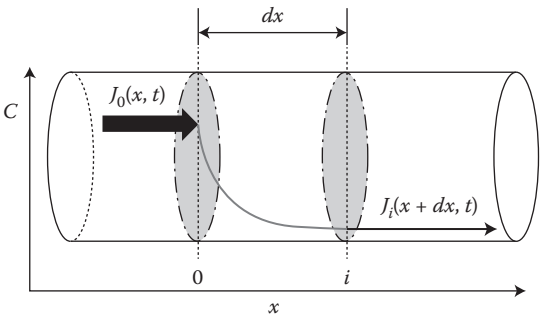

FIGURE 3.9 Picture of Fick's law showing the change in flux with changing concentration and distance. (Reproduced from Setterfield-Price, B. M. *Electrochemical Reduction of Carbon Dioxide*, 2013. With permission from ProQuest ILC.)

techniques have diffusion as the primary form of mass transport and as such D is a useful parameter to define and can be measured experimentally.

3.3.2 Solubility of CO_2

Traditionally, most of the CO_2 reduction research has been carried out in aqueous media. The solubility of CO_2 in aqueous electrolyte is quite low, which results in poor mass transport of CO_2 to the electrode, and is the limitation to obtain high selectivity at high current density. Under moderate experimental conditions, considering CO_2 solubility in water is 30 mM at 1 atm at ambient temperature, the highest current density will be restricted to 20 mA cm^{-2} or so for formation of CO or $HCOO^-$, for example. Such a low transport process must be improved by any means, if the CO_2 reduction is utilized for a practical process. Various solutions have been proposed, such as overcoming by operating at elevated pressure, decreased temperature, in alternate organic media, or using 3D electrodes, such as gas diffusion electrodes (GDEs), solid polymer electrolytes, and packed-bed electrodes. As reported, the solubility of CO_2 in water increases with the decrease in temperature (Table 3.4), for example, 0.058 mol L^{-1} at 269 K compared with 0.033 mol L^{-1} at 298 K under ambient pressure. At 60 atm and 25°C, the solubility of CO_2 in water is over 1 mol L^{-1}. Solubility is also increased through alteration of the solvent system. In methanol, the solubility of CO_2 is over 1 mol L^{-1} at 25°C and 8 atm, a considerably lower pressure than that required to maintain an equivalent concentration in an aqueous system.

The solubility of CO_2 is of great importance for developing the process of ERC because it determines the concentration of CO_2 in the liquid phase (CO_2(aq)), which affects the rate of CO_2 mass transfer to the cathode surface and thus the corresponding product CE.

3.3.3 Influences of CO_2 Mass Transfer Near the Electrode Surface

When CO_2 gas is in contact with an aqueous solution, CO_2 is absorbed into the liquid phase as loosely hydrated CO_2(aq) (Equation 3.33) that subsequently engages in a relatively slow reaction with water to form carbonic acid, H_2CO_3 [51–54].

$$CO_2(g) \rightleftarrows CO_2(aq) \tag{3.33}$$

TABLE 3.4
Solubility of CO_2 in Water (mol/L at 101 kPa CO_2 Partial Pressure)

T, °C	15	25	35	45	55	65	75	85	100
S	0.0455	0.0336	0.0262	0.0215	0.0175	0.0151	0.0120	0.0090	0.0065

Source: Reproduced from *Progress in Energy and Combustion Science*, 34(2), Bachu, S., CO_2 storage in geological media: Role, means, status and barriers to deployment, 254–273, Copyright 2008, with permission from Elsevier.

$$CO_2(aq) + H_2O \underset{k_{-0}}{\overset{k_{+0}}{\rightleftharpoons}} H_2CO_3(K^{\#}) \tag{3.34}$$

For Equation 3.34, the forward reaction ($k_{+0} = 3.0 \times 10^{-2}$ s^{-1}) is much slower than the reverse reaction ($k_{-0} = 23.7$ s^{-1}) at 298 K. As less than 1% of the dissolved CO_2 is present as H_2CO_3, Reactions (3.33) and (3.34) are combined to give the pseudo-equilibrium:

$$CO_2(g) + H_2O(l) \rightleftarrows H_2CO_3^*(K_0) \tag{3.35}$$

in which $[HCO_3^*] = [CO_2(aq)] + [H_2CO_3]$.

In basic solutions (pH > 7), CO_2(aq) may react directly with OH^-:

$$CO_2(aq) + OH^- \underset{k_{-1}}{\overset{k_{+1}}{\rightleftharpoons}} HCO_3^- \quad K_1' \tag{3.36}$$

where the forward reaction ($k_{+1} = 8.5 \times 10^3$ M^{-1} s^{-1}) is much faster than the reverse reaction ($k_{-1} = 2.3 \times 10^{-4}$ s^{-1}) at 298 K.

The rate of CO_2 absorption into the catholyte is determined by the rates of Reactions (3.34) and (3.36) and greatly affected by the physical diffusion rate of CO_2 (Equation 3.33, mass transfer step) through the boundary layers at the gas/liquid (G/L) interface, which is strongly influenced by the way CO_2 gas is contacted with the liquid.

Combining Equations 3.33, 3.34, and 3.35 gives the mass transfer step as the following equation shows [55,56]. Equations 3.34 and 3.36 are the two thermochemical reaction paths that consume CO_2(aq) [56]:

Mass transfer step: A. $CO_2(g) + H_2O(l) \rightleftharpoons CO_2(aq) + H_2O(l) \equiv H_2CO_3^*$

Chemical reactions steps: B. $CO_2(aq) + H_2O \underset{k_{-0}}{\overset{k_{+0}}{\rightleftharpoons}} H_2CO_3 \rightleftharpoons H^+ + HCO_3^-$

C. $CO_2(aq) + OH^- \underset{k_{-1}}{\overset{k_{+1}}{\rightleftharpoons}} HCO_3^-$

For the mass transfer step A, the rate is given by

$$MT_{rate} = k_{G/L} a p_{CO_2} K_0 \tag{3.37}$$

where:

$k_{G/L}$ = the mass transfer coefficient (m s^{-1})
a = the specific G/L surface area (m^2 m^{-3})
p_{CO_2} = the CO_2 partial pressure (kPa)
K_0 = the equilibrium constant for Equation 3.35, that is, 2.94×10^{-4} M^{-1} s^{-1} M kPa^{-1} at 298 K [55].

For the thermochemical reaction steps, for pH < 8, step B dominates and the chemical reaction rate is

$$-\frac{d[CO_2(aq)]}{dt} = k_{+0}h_L\varepsilon[CO_2(aq)] = 3\times10^{-2}h_L\varepsilon[CO_2(aq)] \tag{3.38}$$

where:

k_{+0} = rate constant of reaction 3.34 (s^{-1})
h_L = liquid hold-up (–)
ε = voidage of the 3D cathode (–)
$[CO_2(aq)]$ = concentration of dissolved CO_2 in the catholyte (M).

At pH > 10, step C is predominant and the rate of $CO_2(aq)$ consumption is

$$-\frac{d[CO_2(aq)]}{dt} = k_{+1}h_L\varepsilon[CO_2(aq)][OH^-] = 8.5\times10^{3}h_L\varepsilon[CO_2(aq)][OH^-] \tag{3.39}$$

where:

k_{+1} = rate constant of reaction 3.36 (s^{-1}).

In the pH range of 8–10, both steps are important, hence the rate should be

$$-\frac{d[CO_2(aq)]}{dt} = (3.0\times10^{-2} + 8.5\times10^{3}[OH^-])h_L\varepsilon[CO_2(aq)] \tag{3.40}$$

Table 3.5 shows the calculated mass transfer rate and total thermochemical reaction rates at different pH values where CO_2 partial pressure and temperature are 145 kPa and 298 K, respectively.

Comparing the mass transfer and thermochemical reaction rates, it may be seen that when a catholyte solution of carbonate or of low ratio of bicarbonate/carbonate is fed, that is, pH is higher than about 10, the chemical reaction is so

TABLE 3.5
Estimated Mass Transfer and Thermo-Chemical Reaction Rates at Different pH

pH	7.5	8.5	9.5	10.5
Mass transfer rate (M s^{-1})	0.025			
Chemical reaction rate (M s^{-1})	0.0003	0.0006	0.003	0.03

Source: Reproduced from Li, H. Development of a continuous reactor for the electrochemical reduction of carbon dioxide. 2006. With permission from ProQuest ILC.

Note: Assuming a = 7000 m^2 m^{-3}, h_L = 0.5, ε = 0.5, $k_{G/L} = 1\times10^{-4}$ m s^{-1}.

fast that one cannot expect to have both a relatively high concentration of CO_2(aq) and high bulk pH simultaneously. Hence, depending on the CO_2 pressure, G/L mass transfer capacity, liquid hold-up, and cathode voltage, the catholyte feed solution should have a pH lower than about 10 and a buffer capacity to maintain the bulk catholyte pH less than 10 throughout the reaction. The CO_2(aq) concentration and pH at the reactive cathode surface depend on these bulk conditions, coupled with the current density and L/S mass transfer coefficient, as detailed in Reference 57. Considered along with the equilibria, these mass transfer and thermochemical reaction rates may favor the current density-dependent reduction of CO_2 to formate in the bulk pH range about 7–10 at 298 K. The changes in temperature that occur in a practical case will probably shift this pH window. Kinetic data are not available to calculate the effect of temperature, but applying the rule of thumb, that is, doubling of chemical reaction rates for 10 K increase in T, moves the upper limit of pH down from about 10 to 9 as temperature increases from 298 to 333 K. Apart from the above effects, the electrochemical kinetics of Reactions (3.1) and (3.2) play a major role in determining the formate CE over the whole pH range, and particularly at pH below about 6, where CO_2 sequestration as HCO_3^-/CO_3^{2-} is not an issue.

As mentioned above, there exist overpotentials, or polarizations associated with the mass transport processes. For industrial electrochemical processes, the superficial current density and CE should be, respectively, at least 1 kA m^{-2} and 50%. However, the relatively low solubility of CO_2 in aqueous solutions (ca. 70 mM at STP), coupled with the CO_2(aq)/HCO_3^-/CO_3^{2-} equilibria, creates a mass transfer constraint on the reduction of CO_2. Due to this mass transfer resistance, the resultant current remains very low even at the most active electrocatalyst. The primary current density limits to a maximum value of the order 10 mA cm^{-2} under the typical laboratory reaction conditions (one-phase flow, 2D cathode) with 100 kPa (abs) CO_2 pressure at 298 K. Several devices have been suggested to relieve the CO_2 mass transfer constraint, including operation at super-atmospheric pressure and/or subambient temperature, using a GDE or using a fixed-bed cathode while providing a "3-phase interface" for the reaction by sparging the cathode chamber with CO_2 gas [58–63].

3.4 KINETICS AND CATALYSIS OF CO_2 ELECTROREDUCTION

3.4.1 Steps in CO_2 Electroreduction

As stated, most of the CO_2 electrocatalytic reduction on the surface of an electrode consists of several steps, including mass transfer of the reactants, surface reactions, interfacial charge transfer, and products involving bulk and surface diffusion, forming a complicated system whose components in those different processes affect each other. Each of them may give rise to a polarization phenomenon as discussed above. Figure 3.10 gives the plausible mass transfer at the electrode–electrolyte boundary layer.

Lack of exact rate constants makes the investigation of CO_2 electroreduction mechanisms even more difficult.

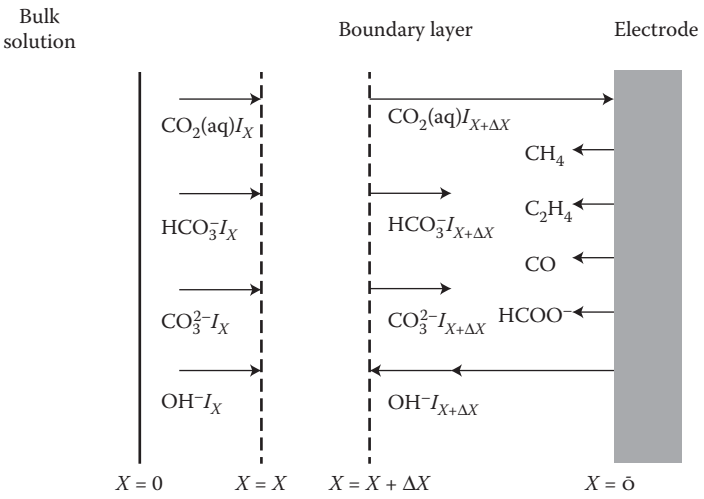

FIGURE 3.10 Mass transfer across the electrode–electrolyte boundary layer. (With kind permission from Springer Science + Business Media: *Journal of Applied Electrochemistry*, Calculation for the cathode surface concentrations in the electrochemical reduction of CO_2 in $KHCO_3$ solutions, 36, 2006, 161–172, Gupta, N., Gattrell, M. and MacDougall, B.)

3.4.2 Dynamic Influences on CO_2 Electroreduction

CO_2 electrochemical reduction is a highly surface-sensitive reaction. The CO_2 coordinates to the metal via either a η^1 or η^2 bond depending upon the identity of the metal and its surface conditions [12,14], to give adsorbed carbon dioxide. The CO_2(ads) then accepts an electron to form the adsorbed radical species, $\cdot CO_2^-$(ads) as mentioned above, from which a number of reaction pathways are possible as discussed below.

In addition, the rates of CO_2 reduction can also be significantly affected within the system by electrolyte size and charge as well. For example, rates increased $Cl^- < Br^- < I^-$ for CO_2 reduction in $MeOH/H_2O$ on Cu [64,65], and rates increased upon moving from Na^+ to La^{3+} in an aqueous Cu system [64].

3.4.3 Turnover Frequency of CO_2 Hydrogenation

The calculated turnover frequency (TOF), as a function of the oxygen adsorption energy, ΔE_O, at ambient pressure and 500 K, is investigated as shown in Figure 3.11 [66]. The optimum in reaction rate is a result of competition between having a too weak interaction with oxygen, resulting in too unstable intermediates and high reaction barriers and a too strong coupling to oxygen, giving rise to surface poisoning by formate, and possibly other species bound through oxygen. As observed, elemental copper is closest to the top, whereas nickel and palladium bind oxygen too strongly and weakly, respectively. Zinc doping in a copper surface step, which can be used to model the active site of $Cu/ZnO/Al_2O_3$ industrial catalysts, [67], have close to

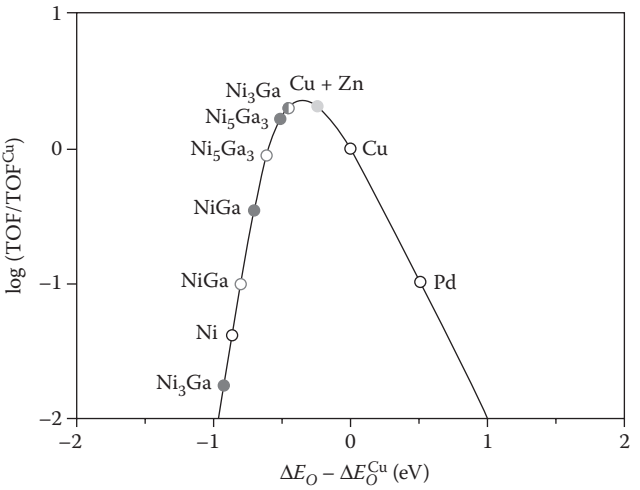

FIGURE 3.11 Theoretical TOF of CO_2 hydrogenation to methanol as a function of ΔE_O, relative to Cu(211). ΔE_O for Ni–Ga intermetallic compounds is depicted as shown in the left side of the curve. Closed circles indicate nickel-rich sites, open circles gallium-rich sites, and half-open circles mixed sites. Reaction conditions: 500 K, 1 bar, and a CO_2:H_2 ratio of 1:3. (Reproduced by permission from Macmillan Publishers Ltd. *Nature Chemistry*, Studt, F. et al. Discovery of a Ni-Ga catalyst for carbon dioxide reduction to methanol. 6(4): 320–324, copyright 2014.)

optimal activity. However, the density of such sites is small in a doped system [67], and a more homogeneous catalyst with the same activity per site but more active sites would be advantageous. The model, a good description either in theoretical or experimental view, provides a good starting point for discovering potential catalysts.

Generally, commercial electrochemical processes typically run at a turnover rate of about 1–10 per second.

3.4.4 Reaction Kinetics and Mechanism of CO_2 Electroreduction

3.4.4.1 Metal Electrodes

Although there is no general consensus on the mechanism for hydrogenation at Cu/ZnO catalysts, Cu(I) sites are thought to promote catalytic activity and selectivity toward CH_3OH. Although Cu–Zn alloys are considered active sites for CO_2 reduction, Cu(I) sites are considered key species for CO adsorption in hydrogenation reactions [68]. Further, Cu(I) sites are believed to stabilize reaction intermediates such as carbonates (CO_3^{2-}-), formates ($HCOO^-$-), and methoxy adsorbates (H_3CO^--) due to their higher heats of adsorption [69]. Sheffer et al. showed that alkali metals help stabilize Cu(I) active sites and increase Cu(I) concentrations which significantly improve CH_3OH yield [70]. Oxidation studies at single crystal Cu(I) shows that H_3CO adsorbed at (111) surfaces with Cu(I) atoms at the second atomic layer allows coordinately unsaturated oxygen anions to act as hydrogen abstraction sites

for dehydrogenation [71]. In this case, it is possible that the unsaturated oxygen atoms at the (111) surfaces of the cuprous oxide film act as hydrogen donors sites in the reduction reaction.

A theoretical report by Peterson et al. describes a pathway for the electrochemical reduction of CO_2 to CH_4 at Cu electrodes based on density functional theory (DFT) and computational hydrogen electrode (CHE) models applied to Hori's experimental data [72]. In that work, the authors indicate that the carbon atom of CO adsorbates may be hydrogenated via proton transfer to form HCO at −0.74 V (RHE). Hydrogenation of an adsorbed CO species is proposed to occur directly via proton addition from solution as their availability is significantly greater than hydrogenation from adsorbed hydrogen. Accordingly, once the HCO species is formed, the carbon atom continues proton and electron transfer reactions to form H_3CO adsorbates. Following this pathway, the last proton transfer to the H_3CO species (on Cu(211) surfaces) favors CH_4 formation by 0.27 eV. In the case of cuprous oxide electrodes as described here, the reduction reaction may benefit from both improved intermediate stability and the ability of H^+ species coordinated with surface-bound oxygen. This surface would allow hydrogen addition to the oxygen atom of the H_3CO adsorbate rather than the carbon atom as shown in Figure 3.12 [73].

The formation of HCO^- intermediate has been reported as the r.d.s. in CO_2 reduction to CH_4, and H_2CO^- intermediate is detected in both hydrogenation and photoelectrocatalytic process for CH_3OH formation [72,74]. Two possible mechanism pathways (a and b) for the direct electrochemical reduction of CO_2 to CH_3OH at Cu/ZnO catalyst are proposed in Figure 3.13 [73]. Although mechanism (a) proceeds through CO pathway, mechanism (b) undergoes formate ($HCOO^-$) intermediate. The last four steps in both (a) and (b) mechanism pathways are the same with HCO adsorbate formation, H_2CO adsorbate formation, H_3CO adsorbate formation, and hydrogenation of H_3CO adsorbate to CH_3OH.

Pathway (a) proceeds via CO intermediate, similar to Peterson and Gattrell's mechanisms for CO_2 reduction at Cu surfaces [72,75]. The first electron and proton transfer may be associated with the formation of dioxymethylene ($HOCO^-$). When another electron and proton are added to the OH group of the $HOCO^-$ adsorbate, the C–OH_2 bond is broken to desorb a H_2O molecule and leave CO adsorbate on the surface. The reaction continues with the formation of HCO species by H addition to the C atom. Once the HCO species are formed, the carbon atom continues proton and electron transfer reactions to form H_2CO and H_3CO adsorbates. Although it is not

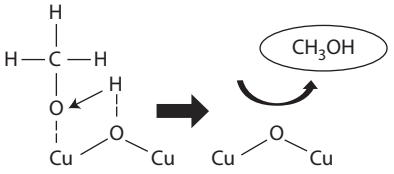

FIGURE 3.12 Hydrogenation of methoxy adsorbates at $Cu_2O(111)$ surfaces. (Le, M. T. H. *Electrochemical Reduction of CO_2 to Methanol*. Louisiana State University, 2011. Reproduced by permission of The Royal Society of Chemistry.)

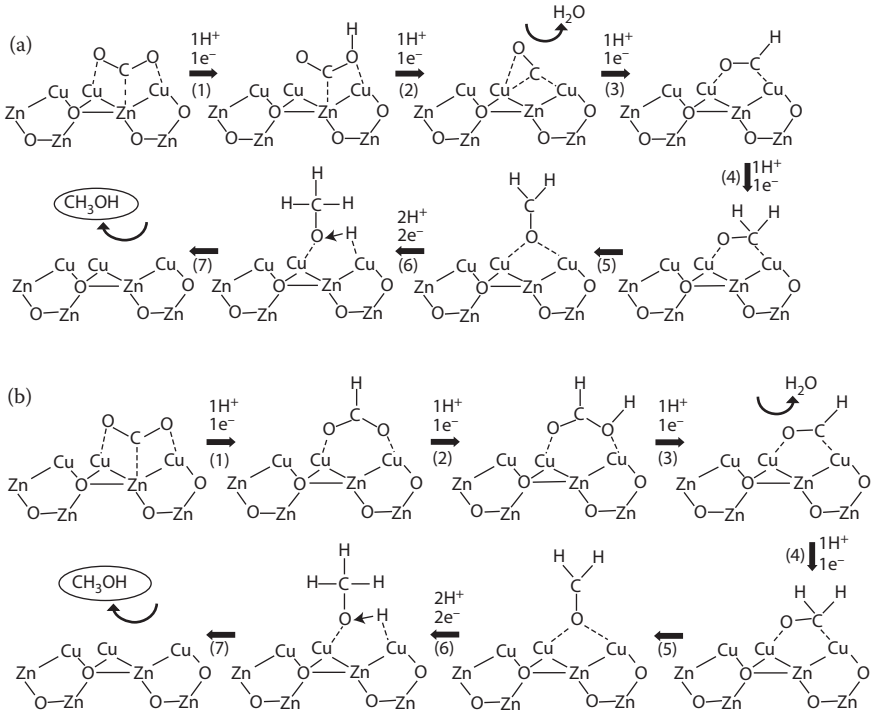

FIGURE 3.13 Proposed mechanisms through CO pathway (a) and $HCOO^-$ intermediate (b) for direct electrochemical reduction of CO_2 to CH_3OH using Cu/ZnO catalyst. (Le, M. T. H. *Electrochemical Reduction of CO_2 to Methanol*. Louisiana State University, 2011. Reproduced by permission of the Royal Society of Chemistry.)

clear whether these adsorbates would attach to the Cu, Zn, or O bond, ZnO (10–10) surface would promote CH_3OH formation by drawing OH adsorption and allowing the H atom to attach to the O atom of the H_3CO species.

Pathway (b) proceeds via $HCOO^-$ intermediate [74]. The H attaches to the C atom instead of the O atom on CO_2 adsorbate, hence, forming $HCOO^-$ rather than $HOCO^-$. The mechanism proceeds with H additions to the O atom of the formate (HCOO) species first to form HCO after an H_2O molecule dissociates from the surface. Similar to mechanism (a), once HCO species are formed, the reaction continues electron and proton transfer until CH_3OH is desorbed from the surface.

In Hg, Tl, Pb, In, Sn, and Cd at aqueous solution, the formation of $HCOO^-$ may be initiated by one electron transfer to CO_2 at the potential negative of –1.6 V vs. SHE, forming $\cdot CO_2^-$ present mostly freely in the solution close to the electrode as depicted in Figure 3.14 (1). The hydrogen bond by water molecules [76] and the high dielectric constant of water molecule contribute to the stabilization of $\cdot CO_2^-$ in solution. The concentration of $\cdot CO_2^-$ would be ca. 10^{-5} mol dm^{-3}, if one takes into account the standard potential –1.85 V or –1.90 V and the Nernst relation 59 mV $decade^{-1}$ at 25°C. Free $\cdot CO_2^-$ will take a proton at the nucleophilic carbon atom from a H_2O molecule

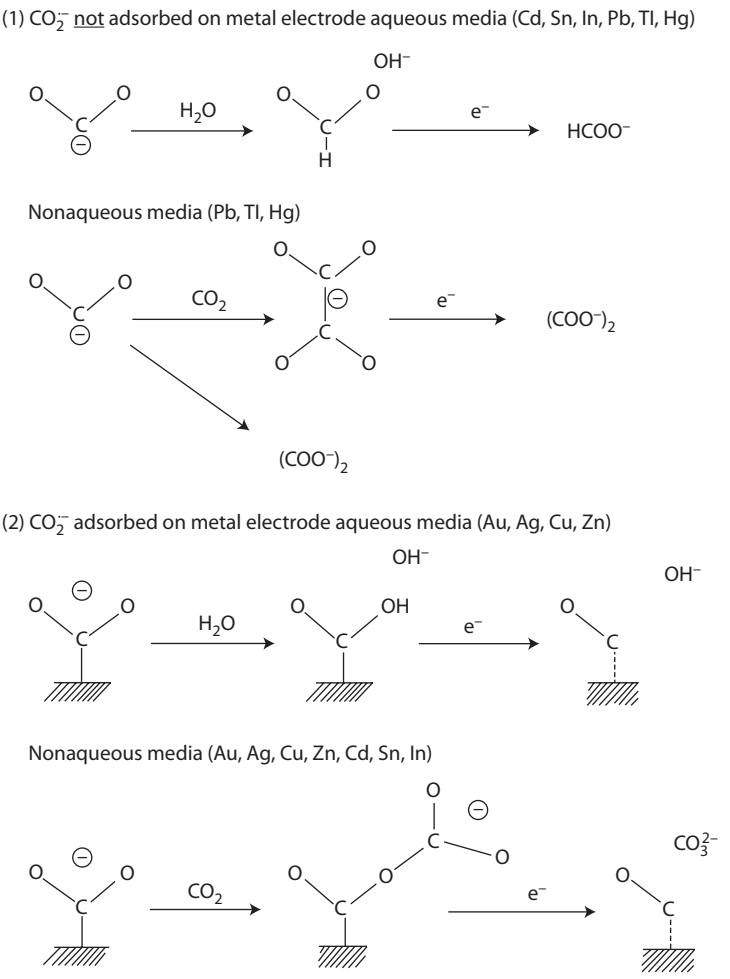

FIGURE 3.14 Reaction scheme of the electrochemical reduction of CO_2. (Reproduced from the *Electrochimica Acta*, 39, Hori, Y. et al. Electrocatalytic process of CO selectivity in electrochemical reduction of CO_2 at metal electrodes in aqueous media, 1833–1839, Copyright 1994, with permission from Elsevier.)

acting as a Lewis acid, forming HCO_2. H^+ will not be bonded to the O atom of $\cdot CO_2^-$ because pKa value of the acid–base couple ($\cdot CO_2^-/CO_2H$) is low at 1.4 [77]. $HCO_2\cdot$; is subsequently reduced to $HCOO^-$ at the electrode in aqueous media. The electrode potentials of Pb, Cd, and Tl are –1.6 V or more negative at 5.0 mA cm^{-2} [31]. The potential of Hg is –1.51 V at 0.5 mA cm^{-2}, which would be equivalent to –1.7 V at 5.0 mA cm^{-2} with an assumption of the transfer coefficient for $HCOO^-$ formation 0.25 [5,9,65]. In nonaqueous media, H_2O molecule is not available and plenty of CO_2 is present. A CO_2 molecule will play a role of a Lewis acid with the nucleophilic C of $\cdot CO_2^-$. The coupling of $\cdot CO_2^-$ and CO_2 will lead to the formation of an adduct

intermediate $\cdot(CO_2)_2^-$, thus producing oxalate [76], which is more probable than Savéant's coupling mechanism [78]. By contrast, CO is produced by a mechanism different from $HCOO^-$ formation which may proceed with free $\cdot CO_2^-$ intervening. CO is favorably produced from the electrode metals which stabilize $\cdot CO_2^-$ effectively.

On the metal electrode surface of Au, Ag, Zn, Pd, Ga, or Cu, giving CO as the major product, $\cdot CO_2^-$ is stabilized by adsorption both in aqueous and nonaqueous electrolytes. Electrophilic reagents, H_2O in aqueous solution, react with the O atom of adsorbed $\cdot CO_2^-$, forming CO(ad) and OH^- as depicted in Figure 3.14 (2). H^+ will not take part in the CO formation as the partial current of CO formation is independent of pH. CO(ad) is readily desorbed from the electrode as a gaseous molecule. The sequence of CO selectivity roughly agrees with that of the electrode potentials shown in Table 3.2. In nonaqueous media, a CO_2 molecule reacts as a Lewis acid with adsorbed $\cdot CO_2^-$, and allows a C–O bond of the $\cdot CO_2^-$ to be broken. This process forms CO(ad) and $\cdot CO_2^-$ as postulated by Hammouche and his coworkers [79] for electrochemical reduction of CO_2 catalyzed by iron porphyrins. CO(ad) thus formed is easily desorbed, as shown in Figure 3.14 (2). Cd, Sn, and In, of medium CO selectivity, do not strongly adsorb $\cdot CO_2^-$. $\cdot CO_2^-$ will be most freely present in aqueous electrolyte owing to the stabilization by water molecules over hydrogen bond [76] and the high dielectric constant. $\cdot CO_2^-$ stabilized in the electrolyte will be further reduced to $HCOO^-$. However, $\cdot CO_2^-$ is not sufficiently stabilized in nonaqueous electrolyte due to lack of hydrogen bond formation and low dielectric constant of the solvents. Thus, $\cdot CO_2^-$ adsorbed on Cd, Sn, and In may be relatively more stable than $\cdot CO_2^-$ dissolved in the electrolyte. These metals yield CO in nonaqueous media in the same manner as Au, Ag, and Zn in Figure 3.14 (2). The CO selectivity mentioned above will be closely connected to the stability of adsorbed $\cdot CO_2^-$ on the electrode.

In H_2O–DMF solutions, the electrochemical reduction of CO_2 at Pb and Hg give mainly oxalate or formate, depending on the concentration of H_2O, with scarce formation of CO at relatively low yield [80–82]. It is proposed that an electron transfer to CO_2 molecule initiates the process, forming $\cdot CO_2^-$, which is not adsorbed on Pb, Hg, and Tl, and is freely present in nonaqueous electrolyte solution as well. And the interactions between the electrode and the reactants, intermediates, and products are negligible as the CO_2 reduction at Hg and Pb electrodes proceeds at potentials close to the standard potential of $\cdot CO_2^-/CO_2$ couple. Several competing homogeneous reactions sequentially take place in parallel in the electrolyte solution (Figure 3.15). The product distribution at Pb and Hg electrodes is determined by the current density and the concentration of CO_2 and H_2O [80]. Oxalate is formed by coupling of $\cdot CO_2^-$, Figure 3.15 (1), formate is formed in a way similar to that in aqueous electrolyte, Figure 3.15 (5)(5′), and CO is formed by sequential reactions (2) and (3) or (3′) in Figure 3.15.

3.4.4.2 Molecular Electrocatalysts

In the proposed mechanism of molecular catalyst of $[Ni^{II}cyclam]^{2+}$ complex (structure 1, Figure 3.16), the $[Ni^{I}cyclam]^+$ complex is assumed to play a crucial role as shown in Figure 3.17, and in particular, a $[Ni^{I}cyclam(CO)]^+$ intermediate species has been detected in the course of selective electroreduction of CO_2 to CO in aqueous solution. Fourteen-membered cyclam framework is a crucial prerequisite for the

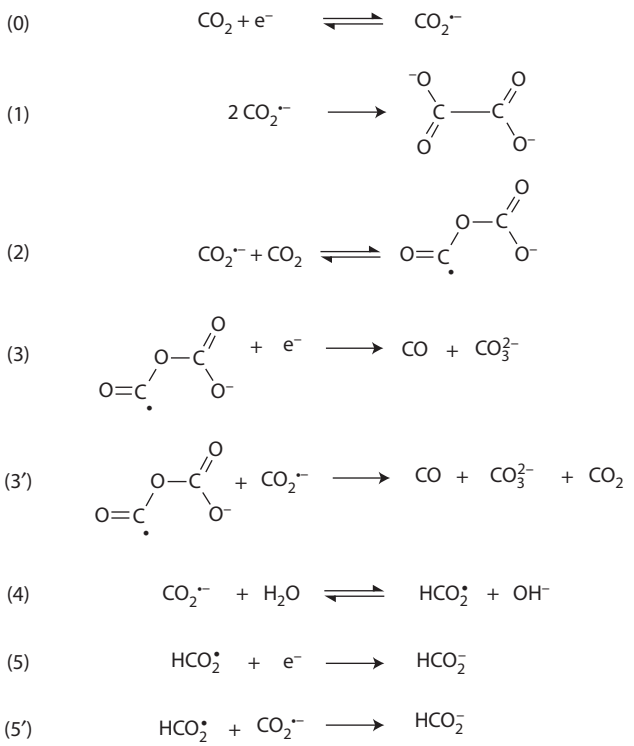

FIGURE 3.15 Reaction scheme of CO_2 reduction without specific interaction between electrode and the reactants, intermediate, and products. (Reproduced with permission from Gressin, J. et al. Electrochemical reduction of carbon-dioxide in low proton media. *Nouveau Journal De Chimie-New Journal of Chemistry*, 3(8–9), 545–554. Copyright 1979 American Chemical Society.)

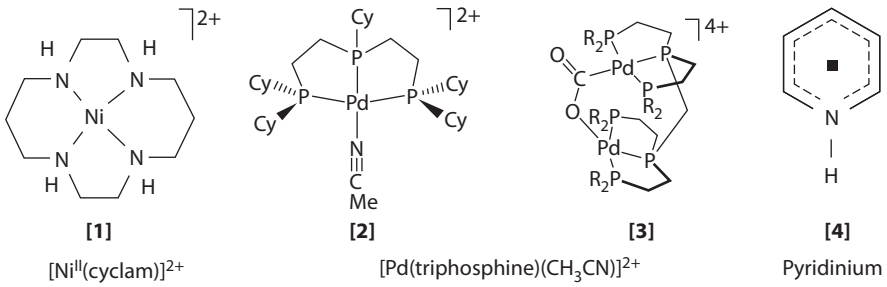

[1] **[2]** **[3]** **[4]**

$[Ni^{II}(cyclam)]^{2+}$ $[Pd(triphosphine)(CH_3CN)]^{2+}$ Pyridinium

FIGURE 3.16 Molecular catalysts of transition metal complexes and nonmetal nitrogen-based pyridimium.

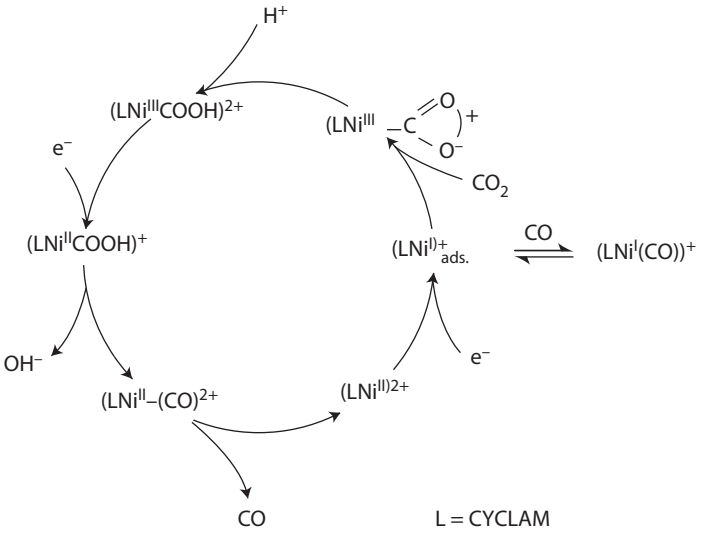

FIGURE 3.17 Postulated mechanistic cycle for the electrocatalytic reduction of CO_2 into CO by Nicyclam^{2+} in water. (Beley, M. et al. Electrocatalytic reduction of carbon dioxide by nickel cyclam2+ in water: Study of the factors affecting the efficiency and the selectivity of the process. *Journal of the American Chemical Society*. 1986; 108(24): 7461–7467. Reproduced by permission of the Royal Society of Chemistry.)

encircled nickel center to act as catalyst in the CO_2 electroreduction. The planar ligand geometry of the Ni(cyclam), allowing access to the metal center, has been suggested to be of significance with respect to the catalytic ability exhibited. The system favors the formation of the Ni^I state [83,84]. [Ni(II)-cyclam] is reportedly a very selective electrocatalyst for CO_2 reduction to CO and was found to catalyze carbon dioxide reduction on mercury electrodes at ca. 0.5 V below the calculated thermodynamic value ($E^0 = -0.41$ V vs. NHE at pH 5) at a "remarkable" velocity of ca. 32 h^{-1} with 95% CO formation CE. The catalyst was reported to cycle more than 1000 times with no notable deactivation. The system was found to be pH dependent, anion specific, prone to deactivation through CO buildup, resulting in Ni(cyclam)(CO) precipitation if the solution is not stirred and reported to require an Hg surface for appreciable rates and turnover [85, 86].

As being developed to date, the most efficient catalyst of modified Fe-porphyrin [87] with phenolic groups in all ortho and ortho' positions on the phenyl groups [88] as depicted in Figure 3.18 was reported to give CO in Faradaic yields >90% through 5×10^7 turnovers over 4 h at an overpotential of just 0.465 V in DMF with 0.2 M water added causing no observable degradation. The enhancement in activity was attributed to the higher local concentration of protons associated with the phenolic hydroxyl groups.

For $[Pd(triphosphine)(CH_3CN)]^{2+}$ catalysts (structure 2, Figure 3.16), the dissociation of a weakly coordinating solvent molecule of acetonitrile favors M–O bond formation during the electrocatalytic reduction cycle of CO_2 to CO. In addition,

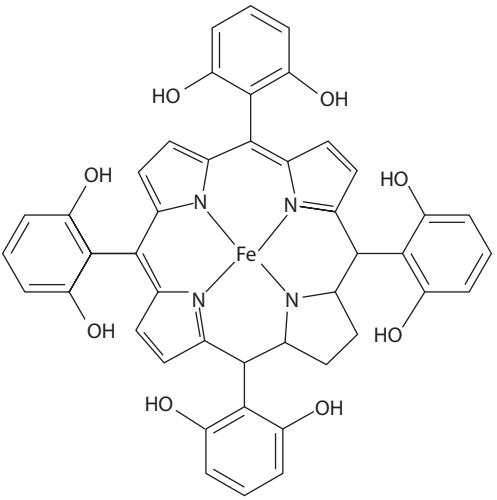

FIGURE 3.18 Iron 5, 10, 15, 20-tetrakis(2′,6′-dihydroxyphenyl)-porphyrin, FeTDHPP. (Costentin, C., Robert, M. and Saveant, J.-M. Catalysis of the electrochemical reduction of carbon dioxide. *Chemical Society Reviews*. 2013; 42(6): 2423–2436. Reproduced by permission of the Royal Society of Chemistry.)

electron-donating substituents on the triphosphine ligand result in increased catalytic rates. The rate constant is between 5 and 300 M^{-1} s^{-1} [89]. The detail catalytic cycle is proposed as shown in Figure 3.19. As the Pd(II) complex gained an electron to form a Pd(I) intermediate, a reaction with CO_2 occurred to form a five-coordinate CO_2 adduct. Upon transfer of the second electron, the Pd(0) intermediate dissociated the solvent. Protonation of one of the oxygen atoms of coordinated CO_2 affords a metallocarboxylic acid intermediate, Pd–COOH. It is believed that the metallocarboxylic acid is protonated again to form a "dihydroxy carbene," and that CO is then formed by dehydration of the dihydroxy carbene. CO dissociation and solvent association regenerates the initial complex. In solutions of high acid concentration, the r.d.s. was found to be the reaction of the Pd(I) intermediate with CO_2, though, in solutions of low acid concentrations, the cleavage of the C–O bond to form carbon monoxide and water limits the rate of the catalytic cycle. These classes of Pd phosphine complexes have shown catalytic rates in the range of 10–300 M^{-1} s^{-1} and with >90% CEs for CO production. Overpotentials were in the range of 100–300 mV, yet turnover numbers were low (ca. 10–100) and the decomposition to Pd(I) dimers and hydrides eventually causes cessation of catalytic activity [85,90,91].

Molecular CO_2 reduction catalyst of binuclear palladium complex (structure 3, Figure 3.16), in which two or more independent Pd triphosphine units $Pd(P_3)$ are incorporated and separated by a methylene spacer, binds CO_2 through two Pd sites, with one metal interacting with C, the other with O. This complex palladium catalysts show very high catalytic rates, increasing by three orders of magnitude, for CO_2 reduction (>104 M^{-1} s^{-1}), but with a turnover number of ca. 10. Along with this increase in catalytic activity came an increase in the formation of Pd(I)–Pd(I) bonds,

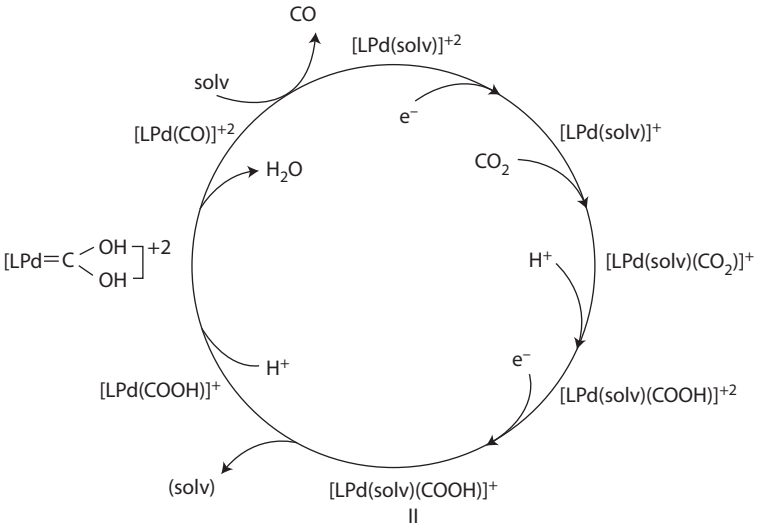

FIGURE 3.19 Proposed catalytic cycle for the Pd^{II} triphosphine complex catalyst. (Benson, E. E. et al. Electrocatalytic and homogeneous approaches to conversion of CO_2 to liquid fuels. *Chemical Society Reviews*. 2009; 38(1): 89–99. Reproduced by permission of The Royal Society of Chemistry.)

thus decreasing catalyst lifetimes. And when the bridge spacer is not methylene, the dendrimers of the Pd catalyst showed decreased activity and selectivity [91].

Studies on the CO_2 reduction to CO by the Re(bpy-R)$(CO)_3$X system (R = H, Me, tBu, X = halogen, OTf, or a neutral ligand with a noncoordinating anion) [93] indicated that the complex undergoes a two-electron reduction and loses the labile X ligand to form an anionic tricarbonyl species (A), reported to be the active form of the catalyst, best described as a Re^0(bpy–R)$^{-1}$ species [94]. The subsequent mechanistic steps are depicted in Figure 3.20. An intermediate of carboxylate species (B) is formed upon reaction of carbon dioxide with the anion (A). The carboxylate species is protonated to form a carboxylic acid species (C), which could then react with a second proton to liberate water and produce a tetracarbonyl cationic intermediate (D). Although the exact order of addition of protons, addition of electrons, and loss of product remain undetermined, the ligand loss and subsequent transfer of electron density to the metal center have been reported as essential steps in the process [93]. The intermediate species involved in catalysis will likely depend on reduction potentials and pKa's of the complexes compared with the applied potentials and pKa's of the Brönsted acids available in solution. TOFs of the bpy-tBu system greater than 250 s^{-1} have been reported [93]. The increasing TOF, compared with that of relatively low value of 21.4 h^{-1} for Re(bpy)$(CO)_3$Cl in DMF–H_2O (9:1) solution, forming CO at –1.49 V vs SCE with CEs at 98% and excellent selectivity over H_2 production [95], attributed to the inclusion of tertiary butyl groups at the 4,4′ positions of the bipyridyl ligand [93] and protic additives to the system [96]. To date, it is one of the best and most well-studied electrocatalyst system of CO_2, still underway almost 30 years on [92].

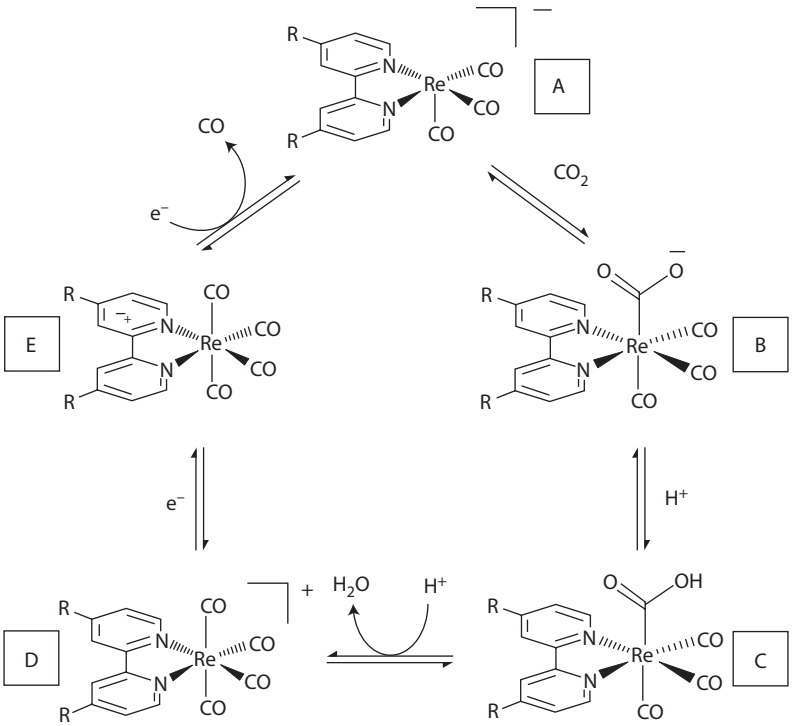

FIGURE 3.20 Proposed mechanism for the catalytic reduction of CO_2 to CO by Re(bpy-R)$(CO)_3X$ species. (Grice, K. A. et al. Carbon monoxide release catalysed by electron transfer: Electrochemical and spectroscopic investigations of [Re(bpy-R)(CO)4](OTf) complexes relevant to CO_2 reduction. *Dalton Transactions*. 2013; 42(23): 8498–8503. Reproduced by permission of The Royal Society of Chemistry.)

The bipyridine complexes of ruthenium, $Ru(bipy)(CO)_2^{2+}$, were found to electrocatalytically reduce CO_2 to CO and $HCOO^-$ at –1.40 V vs. SCE, when water was present [97], by a two-electron reduction process as shown in Figure 3.21 [85,97]. Following the production of CO, a five-coordinate neutral complex is formed. In the presence of CO_2, the complex forms an η^1-CO_2 adduct of Ru(0), which can also be formed by addition of two equivalents of OH^- to $Ru(bipy)(CO)_2^{2+}$. Addition of a proton forms the LRu(CO)(COOH) species which under acidic conditions (pH 6.0) gains another proton to lose water and regenerate the catalyst. Under basic conditions (pH 9.5), the catalyst may undergo a two-electron reduction with the participation of a proton to create $HCOO^-$ and regenerate the five-coordinate Ru(0) complex. The insertion and two-electron attack rely on interactions between the reduced complexes and CO_2 as the electrophile. In this case, both are activated by the occupation of the π^* orbitals of bipyridine. The ligand-based reduction exerts a strong influence on reactivity as electron density at the metal center and in the metal hydride bond is reported as increased making them more susceptible to CO_2 attack. The system is

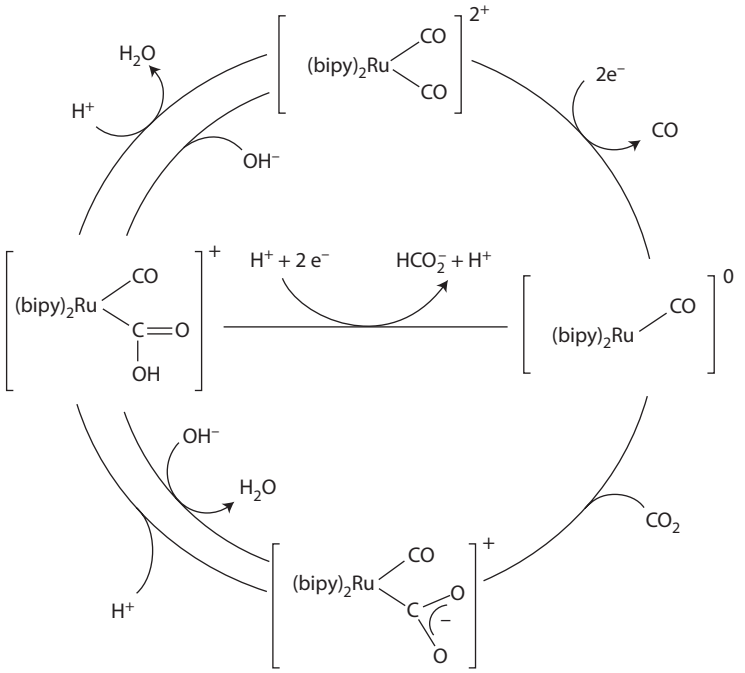

FIGURE 3.21 Proposed mechanism for the catalyst of bipyridine complexes of ruthenium. (Benson, E. E. et al. Electrocatalytic and homogeneous approaches to conversion of CO_2 to liquid fuels. *Chemical Society Reviews*. 2009; 38(1): 89–99. Reproduced by permission of The Royal Society of Chemistry.)

helpful to elucidate several of the key intermediates in the reduction of CO_2, though with low turnover numbers and low selectivity.

cis[Os(bpy)$_2$(CO)H][PF$_6$] reported by Bruce et al. [32] leads to associative activation of CO_2 in nonaqueous solution. At a platinum electrode, the reduction took place at −1.4 to −1.6 V (vs. a NaCl-saturated calomel electrode). The proposed mechanism is illustrated in Figure 3.22. The complex accepts two electrons to give the active species which reacts with CO_2, binding as an extra ligand, leading to coordination sphere expansion. There are different routes proposed where either the initial interaction with the catalyst results in the disproportionation or two of the direduced molecules may combine to give an uncharged complex and disproportionation products, CO and carbonate. In the experiments where water was present, for example, including trace water of less than 10 mM, they reported the incorporation of a proton into the intermediate direduced species, followed by combination to give formate or CO and hydroxide. The complex structure was investigated with the H found *cis* to the carbonyl being swapped for ligands of different sizes, $H > CH_3 > CH_2–C_6H_5 > C_6H_5$. It was seen that the rate constant for the reaction decreased with increasing size of this ligand. The *trans* structure was also trialed as a catalyst but the less sterically demanding configuration was less active. This highlighted the impact of relatively small differences in the molecular structure of the catalyst with a pronounced effect upon catalytic ability seen.

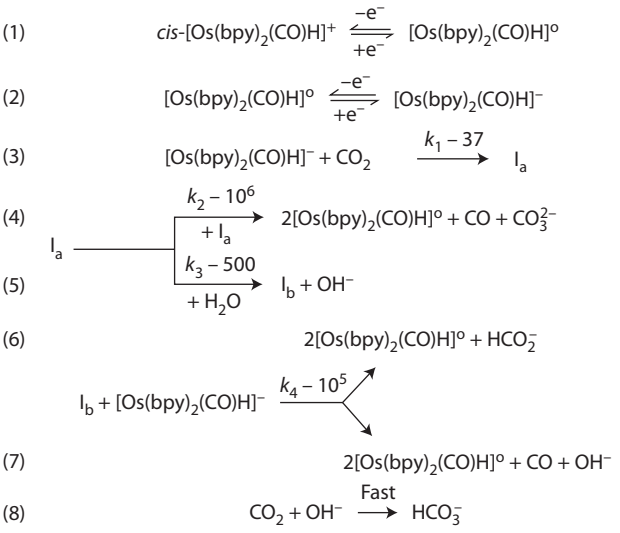

FIGURE 3.22 *cis*$[Os(bpy)_2(CO)H][PF_6]$ catalyst proposed mechanism. (Reproduced with permission from Bruce, M. R. M. et al. Electrocatalytic reduction of carbon dioxide by associative activation. *Organometallics*. 7(1), 238–240. Copyright 1988 American Chemical Society.)

A dinuclear copper(I) complex incorporating pyridyl-like groups was reported to activate and convert CO_2 selectively into oxalate at only a very small applied potential of −0.03 V vs NHE, via a very different and effective catalytic cycle as seen in Figure 3.23. The electrocatalytic reduction of the copper(II) ion to copper(I) appears to be rate limiting, which occurs at a readily accessible potential, around 2 V less negative than that required for CO_2 reduction to $\cdot CO_2^-$ in acetonitrile on a glassy carbon electrode [98]. Two dinuclear direduced copper complexes are thought to form a tetranuclear complex with two bridging CO_2-derived oxalates which are subsequently released as $Li_2C_2O_4$ precipitate. The reduction of CO_2 in this system is found at a significantly less negative potential than that of dioxygen allowing the selective reduction of CO_2 from air. Unfortunately, this catalyst only completed six turnovers with 12 equivalents of oxalate formed in 7 h. So it cannot be considered suitable as a realistic catalyst, yet however is the most efficient route to oxalate in terms of overpotential reported to date [87].

Nonmetal nitrogen-based pyridinium cation (structure 4, Figure 3.16) catalyst [99,100] acts as one-electron shuttle to perform multiple-electron, multiple-proton reduction of CO_2 effectively in aqueous solution with Faradaic efficiencies of methanol observed ~30% at overpotentials of only −0.2 V on metal electrode. When this pyridinium ion catalyst was anchored to a p-GaP electrode, this photochemical system yielded nearly 100% Faradaic efficiency of methanol at potential 0.3 V below the thermodynamic potential of −0.52 V vs SCE for the reaction at pH 5.2 [101]. The detailed mechanism of pyridinium-catalyzed CO_2 reduction in aqueous solution was proposed [99] as given in Figure 3.24. The 6e-reduced product of methanol was

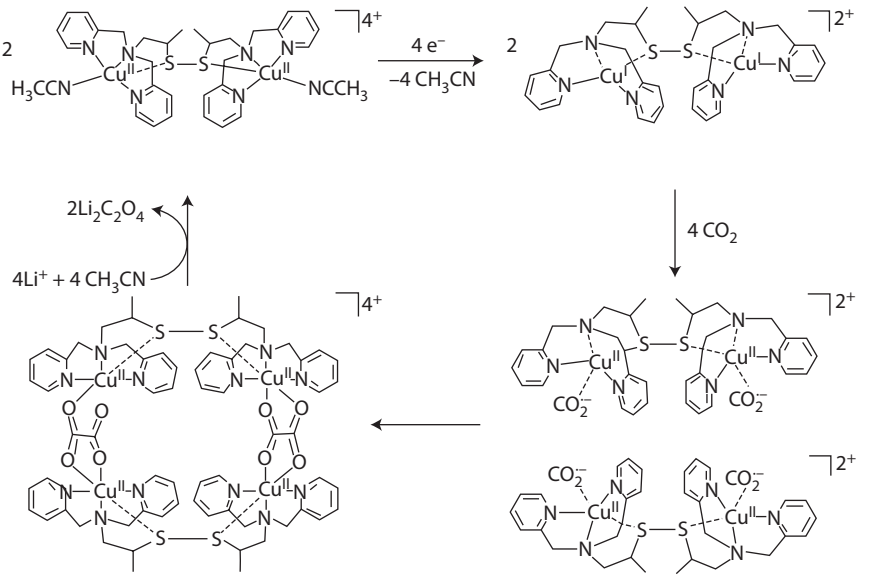

FIGURE 3.23 Proposed mechanism of CO_2 reduction to oxalate by the dinuclear copper complex. (Costentin, C., Robert, M. and Saveant, J.-M. Catalysis of the electrochemical reduction of carbon dioxide. *Chemical Society Reviews*. 2013; 42(6): 2423–2436. Reproduced by permission of the Royal Society of Chemistry.)

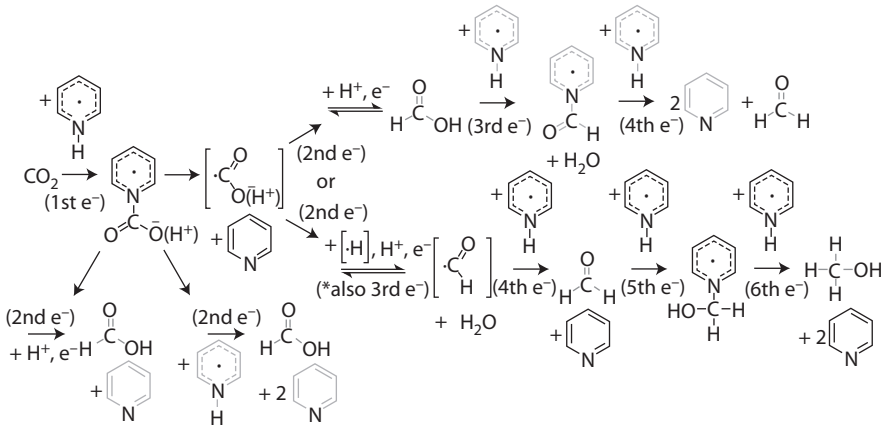

FIGURE 3.24 Overall proposed mechanism for the pyridinium-catalyzed reduction of CO_2 to various products of formic acid, formaldehyde, and methanol. (Reproduced with permission from Barton Cole, E. et al. Using a one-electron shuttle for the multielectron reduction of CO_2 to methanol: Kinetic, mechanistic, and structural insights. *Journal of the American Chemical Society*. 132(33), 11539–11551. Copyright 2010 American Chemical Society.)

through a pathway of a series of single-electron transfer rather than the typical multielectron charge transfer. At metal electrodes, formic acid and formaldehyde were observed to be intermediate products with the pyridinium radical playing a role in the reduction of both intermediate products. The r.d.s. of the aqueous system was reportedly determined as being the initial step, formation of the pyridinum–CO_2 radical.

Large NR_4^+ cations reportedly shift CO_2 reduction to more negative potentials and decrease the associated rate constant as their size increases. This is hypothesized to be the blocking effect of the compact layer of adsorbed cations, perhaps linked to the catalysis by tetraalkylammonium cations on CdTe in DMF and acetonitrile [102,103]. The catalysis was most greatly enhanced by the shorter alkyl chain length with NH_4^+ optimal. The supposed mechanism through which the enhancement was obtained was given as [103]:

1. $NR_4^+ + e^- \rightarrow NR_4^{\cdot}(ads)$
2. $NR_4^{\cdot}(ads) + CO_2(ads) \rightarrow NR_4^+ + \cdot CO_2^-(ads)$
3. $\cdot CO_2^-(ads) + H^+ + e^- \rightarrow CO(ads) + OH^-$
4. $OH^- + H^+ \rightarrow H_2O$

Upon addition of crown ether catalysts with ring structures in the solution, the tetraalkylammonium species, best able to fit within the cavity, yielded higher catalytic activity. The additional lowering of the overpotential in this case was thought to be a result of a similar mechanism as mentioned above, with the crown ether allowing the ammonium ion to get closer to the electrode surface, which is of specific adsorption in the inner Helmholtz plane, rather than outer Helmholtz, increasing the rate of electron transfer to the NR_4^+ species [103].

3.4.4.3 Electrocatalytic Activity Degradation

The reduction of CO_2 at Cu is inefficient, occurring at high overpotentials toward most probable products of hydrocarbons, and the activity drops rapidly as well [4,104–107]. The proposed mechanisms for the activity degradation include adsorption of organic intermediate [105,106], black carbon deposition [105,108], poison of copper oxide patina [107], accumulation of an unknown low vapor pressure and soluble CO_2 reduction product [109], and contaminants Fe^{2+} and Zn^{2+} deposition [4]. However, the real reason behind this is still unclear. The formation mechanism [110] of hydrocarbons [111] is still of a great challenge, though a good start of simulating elements of the reaction mechanism on Cu using DFT [72,112,113]. It is worth noting that Cu electrodes containing a Cu_2O surface layer demonstrated high activity toward CH_3OH production [114,115]. Cu(I) species was considered to play a critical role in the activity of CH_3OH formation. CH_3OH yielded qualitatively follow Cu(I) concentrations.

3.5 PRODUCT DISTRIBUTION AND COMPETITIVE REDUCTION BETWEEN CO_2 AND SOLVENT

3.5.1 Product Distribution

There is a variety of possible product distributions as various pathway steps are involved in different experimental conditions, though a preference occurs for special

occasion. It is noted that small changes can lead to competitive reactions and different routes. Those make generalizations based on individual studies very dubious and grouping difficult.

The reduction product at an electrode in aqueous electrolytes depends on anionic and cationic species of the electrolyte solution, the applied potential, and temperature as discussed. It is reported that CO and $HCOO^-$ were preferentially produced at less negative potentials of >– 0.4 V vs. Ag/AgCl, whereas CH_4, C_2H_4, and C_2H_5OH were major products at the potential <– 0.4 V vs. Ag/AgCl. The origin of the selectivity was hypothesized to relate to the special affinity of hydrogen and/or proton to electrodes. For example, at more negative potential, protons are so abundant on the electrode surface that adsorbed hydrogen-containing carbon molecules are preferentially formed on an Ag electrode. As a result, hydrocarbonization reactions between H_{ad} and $\cdot CO_2^-$ are possible, yielding CH_4, C_2H_4, and C_2H_5OH. On the contrary, at a less negative potential, desorption of H_{ad} occurs, and adsorbed protons are not abundant enough to promote hydrocarbonization reactions. In this case, CO and $HCOO^-$ are preferentially produced.

3.5.2 Competitive Reduction between CO_2 and Solvent

Higher pH solution increases the presence of "H" on the electrode and the amount of carbon dioxide in solution; therefore, electrodes with low affinity for hydrogen adsorption such as aluminum will exhibit optimum CO_2 reduction kinetics at high pH but for others (e.g., palladium) the stronger M–H bonds will mean that H(ads) will dominate the electrode surface, inhibiting CO_2 reduction.

In general, to promote CO_2 reduction reaction while suppressing the competing HER, an electrocatalyst capable of mediating multiple electron and proton transfers at relatively low overpotentials is desirable [111,116–118].

In, Sn, Hg, and Pb electrodes, all have high overpotential for H_2 evolution, and negligible CO adsorption. In aqueous electrolyte, formic acid/formate is selectively produced with Faradaic efficiency between 70% and 100% [23,58,61,119–121].

d group metals (e.g., Pt, Pd, Ru, Fe, Cr, Mo, Ti, Nb, and Ni) have low activity to CO_2 reduction while H_2 evolution dominates. For example, on Ni electrodes, only CO, HCOOH, CH_4, and C_2H_4 with Faradaic efficiency less than 1% were detected in the aqueous electrolyte [120]. On Pd electrodes, CO and HCOOH are the main products from CO_2 reduction, with maximum Faradaic efficiency <30% for both products [31,120]. Under high pressure, for example, 30 atm, the Faradaic efficiency of CO and HCOOH became comparable with that of H_2 [122]. Interestingly, small yield of methanol was reported on Ru electrode [123,124]. Reduction of CO_2 on alloy Ru–Pd (1:1) mainly produced HCOOH with a maximum Faradaic efficiency of 90% [125]. CO_2 is reduced to adsorbed CO (CO_{ad}) on Pt catalysts, the activity of which remarkably depends on the symmetry of the single crystal surface. The following activity series are obtained for stepped surfaces: $Pt(111) < Pt(100) < Pt(S) - [n(111) \times (100)] < Pt(S) - [n(100) \times (111)] < Pt(S) - [n(111) \times (111)] < Pt(110)$. The initial rate of the CO_2 reduction gets higher with the increase of the step atom density [126]. Moreover, kinked step surfaces, which contain protruding atoms along the step lines, have higher activity for CO_2 reduction than the stepped surfaces [127].

The dominance of H_2 evolution could be shifted to CO_2 reduction on d group electrodes by increasing the pressure [120,122]. The formation of hydrocarbons on Cu electrode decreased upon increasing pressure [122,128], whereas lowering the temperature improved the hydrocarbons formation [60,105,120,129,130].

Figure 3.25 shows a result of controlled potential reduction of CO_2 at a Cu electrode in 0.1 M $KHCO_3$. The Faradaic yield of $HCOO^-$, which is thought to be the precursor of the final product of hydrocarbons/alcohols and not reduced at all at a Cu electrode, rises at −0.9 V, reaching maximum at –1.20 to –1.25 V, and drops with the increase of the cathodic potential, whereas H_2 is formed at lower potential with decreasing Faradaic yield along the line.

As shown in Table 3.6, $KHCO_3$, KCl, $KClO_4$, and K_2SO_4 solutions favor the CO_2 reduction. K_2HPO_4 solutions highly promote HER rather than CO_2 reduction at less negative potential. 0.5 M K_2HPO_4 gives much higher H_2 yields than 0.1 M K_2HPO_4. Such an enhancement of HER is attributed to lower pH value at the electrode/electrolyte interface, as mentioned previously. The pH would rise locally at the interface due to OH^- generation in cathodic reactions in aqueous media. Nevertheless, the buffer action of HPO_4^{2-} neutralizes the OH^-, keeping the pH at a lower value. KCl, $KClO_4$, and K_2SO_4 solutions do not have buffer ability, and thus the pH at the electrode/electrolyte interface rises. HER goes up with the concentration of $KHCO_3$ as indicated in Figure 3.26, owing to its buffer action.

In an ionic liquid catholyte of 1-ethyl-3-methyl imidazolium tetrafluoroborate (EMIM-BF4), the conversion of CO_2 to CO over Ag GDE (Figure 3.27) showed substantial improvement over both Faradaic efficiency (~100%) and the overpotential less negative than −0.2 V toward CO formation [29]. The ionic liquid was considered to react with CO_2 to form a complex such as CO_2–EMIM at potentials more negative

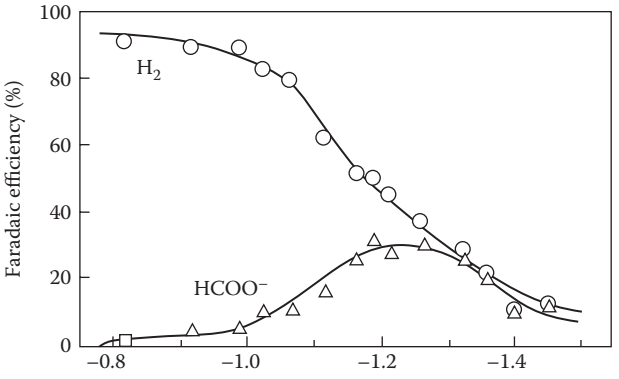

FIGURE 3.25 Variation of the Faradaic efficiencies of different products in electrochemical reduction of CO_2 at a Cu electrode in controlled potential electrolysis, 0.1 mol kg^{-1} $KHCO_3$, 1 atm CO_2, 18°C. (Hori, Y., Murata, A. and Takahashi, R. Formation of hydrocarbons in the electrochemical reduction of carbon dioxide at a copper electrode in aqueous solution. *Journal of the Chemical Society, Faraday Transactions 1: Physical Chemistry in Condensed Phases*. 1989; 85(8): 2309–2326. Reproduced by permission of the Royal Society of Chemistry.)

TABLE 3.6
Faradaic Efficiencies of Products from the Electroreduction of CO_2 at a Cu Electrode at 5 mA cm^{-2} in Various Solutions at 19°C

				Faradaic Efficiency (%)							
Solution	**Concentration, M**	**pH[a]**	**Potential V vs. SHE**	**CH_4**	**C_2H_4**	**EtOH**	**PrOH**	**CO**	**$HCOO^-$**	**H_2**	**Total**
$KHCO_3$	0.1	6.8	−1.41	29.4	30.1	6.9	3.0	2.0	9.7	10.9	92.0
KCl	0.1	5.9	−1.44	11.5	47.8	21.9	3.6	2.5	6.6	5.9	99.8
KCl	0.5		−1.39	14.5	38.2	[b]	[b]	3.0	17.9	12.5	
$KClO_4$	0.1	5.9	−1.40	10.2	48.1	15.5	4.2	2.4	8.9	6.7	96.0
K_2SO_4	0.1	5.8	−1.40	12.3	46.0	18.2	4.0	2.1	8.1	8.7	99.4
K_2HPO_4	0.1	6.5	−1.23	17.0	1.8	0.7	tr	1.3	5.3	72.4	98.5
K_2HPO_4	0.5	7.0	−1.17	6.6	1.0	0.6	0.0	1.0	4.2	83.3	96.7

Source: Hori, Y. et al. Formation of hydrocarbons in the electrochemical reduction of carbon dioxide at a copper electrode in aqueous solution. *Journal of the Chemical Society, Faraday Transactions 1: Physical Chemistry in Condensed Phases*. 1989; 85(8): 2309–2326. Reproduced by permission of The Royal Society of Chemistry.

[a] pH values were measured for bulk solution after electrolysis.

[b] Not analyzed.

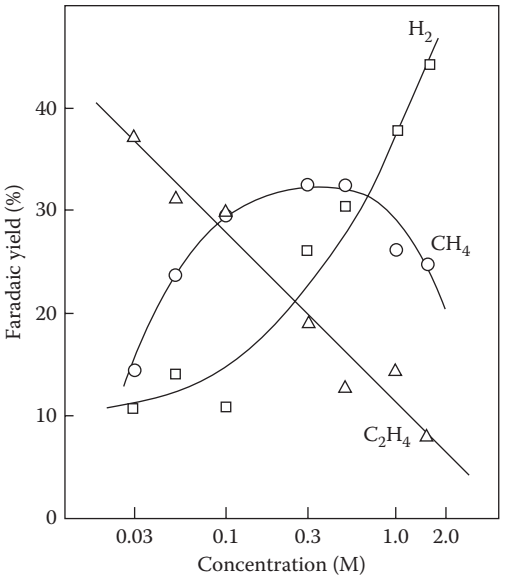

FIGURE 3.26 Faradaic yields of the products in the CO_2 reduction at a Cu electrode at 19°C in $KHCO_3$ aqueous solutions of various concentrations. Current density: 5 mA cm^{-2}. (Hori, Y., Murata, A. and Takahashi, R. Formation of hydrocarbons in the electrochemical reduction of carbon dioxide at a copper electrode in aqueous solution. *Journal of the Chemical Society, Faraday Transactions 1: Physical Chemistry in Condensed Phases*. 1989; 85(8): 2309–2326. Reproduced by permission of the Royal Society of Chemistry.)

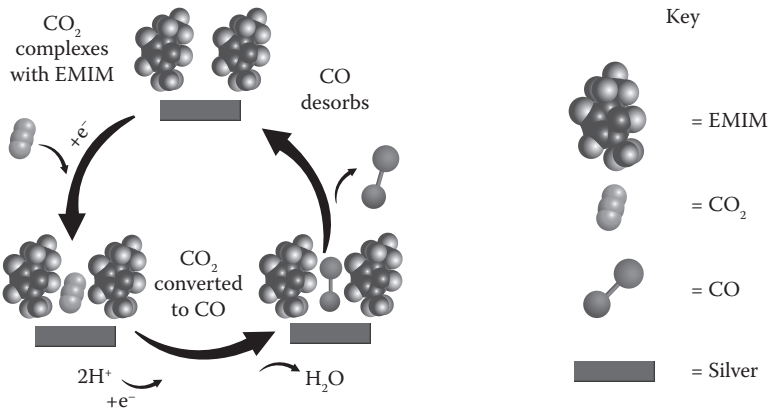

FIGURE 3.27 Plausible CO_2 electrocatalytic reduction pathway in EMIM-BF_4 at Ag electrode. (Reproduced with permission from Rosen, B. A. et al. In situ spectroscopic examination of a low overpotential pathway for carbon dioxide conversion to carbon monoxide. *The Journal of Physical Chemistry C*. 116(29): 15307–15312. Copyright 2012 American Chemical Society.)

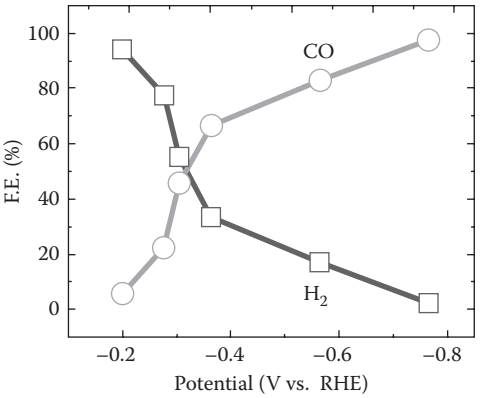

FIGURE 3.28 CO and H_2 Faradaic efficiency at different applied potentials for bulk MoS_2 in CO_2-saturated 96 mol% water and 4 mol% EMIM-BF_4 solution (pH = 4). (Reproduced by permission from Macmillan Publishers Ltd. *Nature Communications*, Asadi, M. et al. Robust carbon dioxide reduction on molybdenum disulphide edges. 5: 4470, copyright 2014.)

than −0.1 V with respect to SHE. This complex substantially lowered the barrier for formation of the intermediate $\cdot CO_2^-$ and suppressed H_2 evolution [131].

For MoS_2 catalysts in the electrolyte of 96 mol% water and 4 mol% EMIM-BF_4 at applied potentials between −0.2 and −0.764 V, both CO_2 reduction to CO and HER on the electrode surface are observed as shown in Figure 3.28 [132]. The measured FE of the CO and H_2 formation, ranging from 0% to ~100% in each component, strongly depends on the applied potential, probably attributed to the difference in the mechanisms of CO_2 reduction and HER. At low overpotential, H_2 is predominantly produced as the favorable thermodynamic potential for the H_2 evolution is low compared with CO_2 reduction. However, when the applied potential exceeds the onset potential of −0.164 V at this system for the CO_2 reduction, CO_2 reduction reaction is activated and dominated instead of HER, in which two H^+ from the electrolyte per one CO_2 molecule reduction are consumed for CO formation, coupled with the electron transfer on the catalyst surface [40,75,133,134].

3.6 SUMMARY AND CHALLENGES

Although the electrochemical conversion of CO_2 has great potential, significant technological advances are still needed for this process to become economically viable. There are three criteria [135]: (1) high energy efficiency, (2) high current density (i.e., high reaction rate or turnover number), and (3) long-term stability. So far, the development of electrochemical reduction of CO_2 system is slow due to the lack of scientific understanding of CO_2 reduction mechanism (C–O, C–C, and C–H bonds formation), pathways and intermediates to generate useful products, providing insights into the CO_2 reduction chemistry at the electrode/electrolyte interface and the degradation mechanism of Faradaic efficiency, although some attempts to

understand the CO_2 electroreduction process through both experimental and theoretical modeling approaches. Such efforts in fundamental mechanistic studies will guide the development of new catalysts and the optimization of operating conditions.

High energetic efficiency can be achieved through a combination of high selectivity (Faradaic or CE) and low overpotentials (Figure 3.29).

Typically, the Faradaic efficiency for many products is >90% for formic acid and carbon monoxide, 65%–70% for methane and ethylene, respectively. High overpotentials are a major hindrance to improving energy efficiency. The reaction rate, as measured by the current density, is also an important parameter as it determines the reactor size and thus capital cost of the process. To date, researchers have reported moderate-to-high current densities (200–600 mA/cm^2) using GDEs similar to those used in fuel cells.

The limiting step in the reduction of CO_2 is the formation of a $\cdot CO_2^-$ radical anion intermediate. (In this context, "CO_2^-" does not necessarily denote a bare $\cdot CO_2^-$ anion; instead, it is whatever species forms when an electron is added to CO_2.) The equilibrium potential for $\cdot CO_2^-$ formation is very negative in water and in most common solvents [103,136] as discussed above, and this is the reason for the high overpotentials [11,29]. This potential can be improved by stabilizing the intermediate, which is one of the main functions of catalysts. Research has shown that the potential to form this radical anion can be improved by 0.3 V by adsorbing it on a catalyst surface [11]. Further improvements could be possible through optimization of the catalyst.

Another key limiting factor in CO_2 conversion is mass transfer of CO_2 to the cathode surface, especially given the low solubility of CO_2 in many electrolytes. As mentioned earlier, this has largely been overcome using GDEs, which create a three-phase interface between the gaseous reactants, the solid catalyst, and the electrolyte.

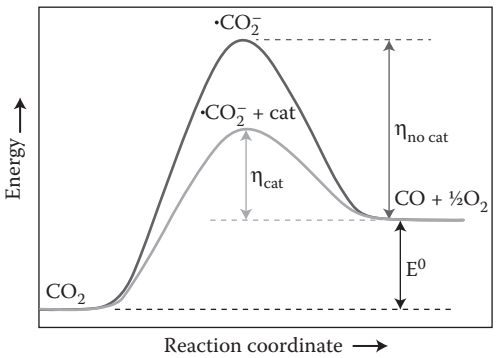

$$\varepsilon_{Faradaic} = \frac{n \cdot F \cdot n}{Q}$$

$$\varepsilon_{energetic} = \frac{E^0}{E^0 + \eta} \times \varepsilon_{Faradaic}$$

Where $\varepsilon_{energetic}$ = energetic efficiency
$\varepsilon_{Faradaic}$ = Faradaic efficiency
n = number of electrons
F = Faraday's constant
n = number of moles of product
Q = charge passed
E^0 = standard potential
η = overpotential

FIGURE 3.29 Qualitative reaction scheme for CO_2 conversion. Catalysts and electrolytes acting as cocatalysts can lower the energy of the intermediate and thus improve the energetic efficiency of the conversion. We use ϵ as the symbol for the Faradaic and energetic efficiencies to avoid confusion with the η symbol for the overpotential. (Reproduced with permission from Whipple, D. T. and Kenis, P. J. A. Prospects of CO_2 utilization via direct heterogeneous electrochemical reduction. *The Journal of Physical Chemistry Letters.* 1(24), 3451–3458. Copyright 2010 American Chemical Society.)

Thus, optimization of the electrode will be a key to improving current densities. The extensive work on GDE optimization for fuel cells over the past decades will greatly accelerate progress in this area.

Although remarkable achievements have been made in electrochemical reduction of CO_2 in the past two decades, there is limited scientific knowledge about CO_2 catalytic reduction. Due to the complexity of the reaction environment and multiple bond-forming and breaking processes, the detailed knowledge about the elementary pathways is obscured, which results in the difficulty in understanding the reaction kinetics and controlling the reaction chemistry. The determination of the transient catalytic intermediates is still not possible because of their very short lifetimes and low concentrations as well as difficulty in resolving intermediates spectroscopically. The characterization of surface intermediates under working conditions will require the development and application of sensitive ultrafast spectroscopic and pump-probe scattering methods. Coupling with the experimental probing, theoretical modeling, such as ab initio methods and DFT, is needed to calculate the overall reaction energies and activation barriers, which subsequently lead to construct overall potential energy surfaces. However, so far, simulating reaction conditions that explicitly treat the effects of surface coverage, electrolyte, electrochemical potential, and appropriate materials property, including the effects of particle size, surface orientation, and morphology, present significant challenges.

More work is needed to further understand the competition between H_2 evolution reaction and hydrogen protonation process. Multiphysical modeling is required to understand the ion (especially H^+) distribution across the buffer layer, the effect of electrolyte circulating rate, cell temperature and reaction gas pressure on the performance.

REFERENCES

1 Yamamoto, T., Tryk, D. A., Fujishima, A. and Ohata, H. Production of syngas plus oxygen from CO_2 in a gas-diffusion electrode-based electrolytic cell. *Electrochimica Acta*. 2002; 47(20): 3327–3334.

2. Seshan, K., Lercher, J., Paul, J. and Pradier, C. Carbon dioxide chemistry: Environmental issues. *The Royal Society of Chemistry.* 1994; 16.

3. Coehn, A. and Jahn, S. Electrolytic reduction of carbon dioxide. *Berichte der Deutschen Chemischen Gesellschaft*. 1904; 37: 2836.

4. Hori, Y., Konishi, H., Futamura, T., Murata, A., Koga, O., Sakurai, H. and Oguma, K. "Deactivation of copper electrode" in electrochemical reduction of CO_2. *Electrochimica Acta*. 2005; 50(27): 5354–5369.

5. Ryu, J., Andersen, T. N. and Eyring, H. Electrode reduction kinetics of carbon dioxide in aqueous solution. *The Journal of Physical Chemistry*. 1972; 76(22): 3278–3286.

6. Kapusta, S. and Hackerman, N. The electroreduction of carbon dioxide and formic acid on tin and indium electrodes. *Journal of the Electrochemical Society.* 1983; 130(3): 607–613.

7. Udupa, K. S., Subramanian, G. S. and Udupa, H. V. K. The electrolytic reduction of carbon dioxide to formic acid. *Electrochimica Acta*. 1971; 16(9): 1593–1598.

8. Sammells, A., Cook, R., Sullivan, B., Krist, K. and Guard, H. *Electrochemical and Electrocatalytic Reactions of Carbon Dioxide*. Elsevier, Amsterdam, 1993.

9. Paik, W., Andersen, T. N. and Eyring, H. Kinetic studies of the electrolytic reduction of carbon dioxide on the mercury electrode. *Electrochimica Acta*. 1969; 14(12): 1217–1232.
10. Kaneco, S., Iiba, K., Hiei, N.-h., Ohta, K., Mizuno, T. and Suzuki, T. Electrochemical reduction of carbon dioxide to ethylene with high Faradaic efficiency at a Cu electrode in CsOH/methanol. *Electrochimica Acta*. 1999; 44(26): 4701–4706.
11. Chaplin, R. P. S. and Wragg, A. A. Effects of process conditions and electrode material on reaction pathways for carbon dioxide electroreduction with particular reference to formate formation. *Journal of Applied Electrochemistry*. 2003; 33(12): 1107–1123.
12. DuBois, D. L. In electrochemical reactions of carbon dioxide. In: Scholz F and Pickett CJ, eds. *Encyclopedia of Electrochemistry*. Wiley-VCH, Weinheim, 2007, pp. 202–224.
13. Hori, Y., Murata, A. and Takahashi, R. Formation of hydrocarbons in the electrochemical reduction of carbon dioxide at a copper electrode in aqueous solution. *Journal of the Chemical Society, Faraday Transactions 1: Physical Chemistry in Condensed Phases*. 1989; 85(8): 2309–2326.
14. Jitaru, M., Lowy, D. A., Toma, M., Toma, B. C. and Oniciu, L. Electrochemical reduction of carbon dioxide on flat metallic cathodes. *Journal of Applied Electrochemistry*. 1997; 27(8): 875–889.
15. Scibioh, M. A. and Viswanathan, B. Electrochemical reduction of carbon dioxide: A status report. *Proceedings of the Indian National Science Academy*. 2004; 70A(3): 407–462.
16. Vassiliev, Y. B., Bagotsky, V. S., Osetrova, N. V., Khazova, O. A. and Mayorova, N. A. Electroreduction of carbon dioxide: Part I. The mechanism and kinetics of electroreduction of CO_2 in aqueous solutions on metals with high and moderate hydrogen overvoltages. *Journal of Electroanalytical Chemistry and Interfacial Electrochemistry*. 1985; 189(2): 271–294.
17. Teeter, T. E. and Van Rysselberghe, P. Reduction of carbon dioxide on mercury cathodes. *The Journal of Chemical Physics*. 1954; 22(4): 759–760.
18. Tryk, D. A. and Fujishima, A. Electrochemists enlisted in war on global warming: The carbon dioxide reduction battle. *The Electrochemical Society Interface*. 2001; 10(1): 32–36.
19. Schwarz, H. A. and Dodson, R. W. Reduction potentials of CO_2^- and the alcohol radicals. *The Journal of Physical Chemistry*. 1989; 93(1): 409–414.
20. Surdhar, P. S., Mezyk, S. P. and Armstrong, D. A. Reduction potential of the carboxyl radical anion in aqueous solutions. *The Journal of Physical Chemistry*. 1989; 93(8): 3360–3363.
21. Lamy, E., Nadjo, L. and Saveant, J. M. Standard potential and kinetic parameters of the electrochemical reduction of carbon dioxide in dimethylformamide. *Journal of Electroanalytical Chemistry and Interfacial Electrochemistry*. 1977; 78(2): 403–407.
22. Pacansky, J., Wahlgren, U. and Bagus, P. S. SCF ab-initio ground state energy surfaces for CO_2 and CO_2^-. *The Journal of Chemical Physics*. 1975; 62(7): 2740–2744.
23. Kaneco, S., Iwao, R., Iiba, K., Ohta, K. and Mizuno, T. Electrochemical conversion of carbon dioxide to formic acid on Pb in KOH/methanol electrolyte at ambient temperature and pressure. *Energy*. 1998; 23(12): 1107–1112.
24. Li, H. and Oloman, C. The electro-reduction of carbon dioxide in a continuous reactor. *Journal of Applied Electrochemistry*. 2005; 35(10): 955–965.
25. Bard, A. J. and Faulkner, L. R. *Electrochemical Methods: Fundamentals and Applications*. 2nd ed. ed: John Wiley & Sons, Inc., New York, NY, p. 100. 2001.
26. Tao, G. Investigation of carbon dioxide electrolysis reaction kinetics in a solid oxide electrolyzer, 2003.
27. Cussler, E. L. *Diffusion: Mass Transfer in Fluid Systems*. Cambridge University Press, Cambridge, 2009.

28. Bockris, J. O. M. and Reddy, A. K. *Modern Electrochemistry: An Introduction to an Interdisciplinary Area*. Springer Science & Business Media, New York, NY, 2012.
29. Rosen, B. A., Salehi-Khojin, A., Thorson, M. R., Zhu, W., Whipple, D. T., Kenis, P. J. A. and Masel, R. I. Ionic liquid–mediated selective conversion of CO_2 to CO at low overpotentials. *Science*. 2011; 334(6056): 643–644.
30. Hori, Y., Murata, A., Kikuchi, K. and Suzuki, S. Electrochemical reduction of carbon dioxides to carbon monoxide at a gold electrode in aqueous potassium hydrogen carbonate. *Journal of the Chemical Society, Chemical Communications*. 1987; (10): 728–729.
31. Hori, Y., Wakebe, H., Tsukamoto, T. and Koga, O. Electrocatalytic process of CO selectivity in electrochemical reduction of CO_2 at metal electrodes in aqueous media. *Electrochimica Acta*. 1994; 39(11–12): 1833–1839.
32. Bruce, M. R. M., Megehee, E., Sullivan, B. P., Thorp, H., O'Toole, T. R., Downard, A. and Meyer, T. J. Electrocatalytic reduction of carbon dioxide by associative activation. *Organometallics*. 1988; 7(1): 238–240.
33. Li, C. W. and Kanan, M. W. CO_2 reduction at low overpotential on Cu electrodes resulting from the reduction of thick Cu_2O films. *Journal of the American Chemical Society*. 2012; 134(17): 7231–7234.
34. Schrebler, R., Cury, P., Herrera, F., Gómez, H. and Córdova, R. Study of the electrochemical reduction of CO_2 on electrodeposited rhenium electrodes in methanol media. *Journal of Electroanalytical Chemistry*. 2001; 516(1–2): 23–30.
35. Frese, J. *Electrochemical Reduction of CO_2 at Solid Electrodes*. Elsevier, Amsterdam, 1993.
36. Noda, H., Ikeda, S., Yamamoto, A., Einaga, H. and Ito, K. Kinetics of electrochemical reduction of carbon dioxide on a gold electrode in phosphate buffer solutions. *Bulletin of the Chemical Society of Japan*. 1995; 68(7): 1889–1895.
37. Lu, Q., Rosen, J., Zhou, Y., Hutchings, G. S., Kimmel, Y. C., Chen, J. G. and Jiao, F. A selective and efficient electrocatalyst for carbon dioxide reduction. *Nature Communications*. 2014; 5: 3242.
38. Hori, Y. Electrochemical CO_2 reduction on metal electrodes. In: Vayenas C, White R and Gamboa-Aldeco M, eds. *Modern Aspects of Electrochemistry*. Springer, New York, 2008, pp. 89–189.
39. Gileadi, E. *Electrode Kinetics for Chemists, Chemical Engineers, and Materials Scientists*. Wiley-VCH Capstone, New York, NY, 1993.
40. Chen, Y., Li, C. W. and Kanan, M. W. Aqueous CO_2 reduction at very low overpotential on oxide-derived Au nanoparticles. *Journal of the American Chemical Society*. 2012; 134(49): 19969–19972.
41. Chen, Y. and Kanan, M. W. Tin oxide dependence of the CO_2 reduction efficiency on tin electrodes and enhanced activity for tin/tin oxide thin-film catalysts. *Journal of the American Chemical Society*. 2012; 134(4): 1986–1989.
42. Chen, Z., Cummins, D., Reinecke, B. N., Clark, E., Sunkara, M. K. and Jaramillo, T. F. Core–shell MoO_3–MoS_2 nanowires for hydrogen evolution: A functional design for electrocatalytic materials. *Nano Letters*. 2011; 11(10): 4168–4175.
43. Kibsgaard, J., Chen, Z., Reinecke, B. N. and Jaramillo, T. F. Engineering the surface structure of MoS2 to preferentially expose active edge sites for electrocatalysis. *Nature Materials*. 2012; 11(11): 963–969.
44. Kim, J. J., Summers, D. P. and Frese Jr, K. W. Reduction of CO_2 and CO to methane on Cu foil electrodes. *Journal of Electroanalytical Chemistry and Interfacial Electrochemistry*. 1988; 245(1–2): 223–244.
45. Atkins, P. and Paula, J. d. *Atkin's Physical Chemistry*. 8th ed. ed: Oxford University Press, Oxford, 2006.
46. Setterfield-Price, B. M. *Electrochemical Reduction of Carbon Dioxide*, 2013.

47. Einstein, A. A new determination of molecular dimensions. *Annals of Physics*. 1906; 19(2): 289–306.
48. Wilke, C. and Chang, P. Correlation of diffusion coefficients in dilute solutions. *AIChE Journal*. 1955; 1(2): 264–270.
49. Harte, C. R. and Baker, E. M. Absorption of carbon dioxide in aqueous sodium carbonate-bicarbonate solutions. *Industrial and Engineering Chemistry.* 1933; 25(10): 1128–1132.
50. Bachu, S. CO_2 storage in geological media: Role, means, status and barriers to deployment. *Progress in Energy and Combustion Science*. 2008; 34(2): 254–273.
51. Keene, F. R., Sullivan, B., Krist, K. and Guard, H. *Electrochemical and Electrocatalytic Reactions of Carbon Dioxide*. Elsevier, Amsterdam, 1993, pp. 1–18.
52. Palmer, D. A. and Van Eldik, R. The chemistry of metal carbonato and carbon dioxide complexes. *Chemical Reviews.* 1983; 83(6): 651–731.
53. Williams, R., Crandall, R. S. and Bloom, A. Use of carbon dioxide in energy storage. *Applied Physics Letters.* 1978; 33(5): 381–383.
54. Walker, A. C., Bray, U. B. and Johnston, J. Equilibrium in solutions of alkali carbonates. *Journal of the American Chemical Society.* 1927; 49(5): 1235–1256.
55. Perry, J. *Chemicals Engineers' Handbook*, 5th ed. ed: McGraw-Hill, New York, 1973.
56. Li, H. *Development of a Continuous Reactor for the Electro-Chemical Reduction of Carbon Dioxide*. University of British Columbia, British Columbia, Canada, 2006.
57. Gupta, N., Gattrell, M. and MacDougall, B. Calculation for the cathode surface concentrations in the electrochemical reduction of CO_2 in $KHCO_3$ solutions. *Journal of Applied Electrochemistry*. 2006; 36(2): 161–172.
58. Mahmood, M., Masheder, D. and Harty, C. Use of gas-diffusion electrodes for high-rate electrochemical reduction of carbon dioxide. I. Reduction at lead, indium-and tin-impregnated electrodes. *Journal of Applied Electrochemistry.* 1987; 17(6): 1159–1170.
59. Todoroki, M., Hara, K., Kudo, A. and Sakata, T. Electrochemical reduction of high pressure CO_2 at Pb, Hg and In electrodes in an aqueous $KHCO_3$ solution. *Journal of Electroanalytical Chemistry*. 1995; 394(1–2): 199–203.
60. Mizuno, T., Naitoh, A. and Ohta, K. Electrochemical reduction of CO_2 in methanol at –30°C. *Journal of Electroanalytical Chemistry*. 1995; 391(1–2): 199–201.
61. Mizuno, T., Ohta, K., Sasaki, A., Akai, T., Hirano, M. and Kawabe, A. Effect of temperature on electrochemical reduction of high-pressure CO_2 with In, Sn, and Pb electrodes. *Energy Sources*. 1995; 17(5): 503–508.
62. Köleli, F. and Balun, D. Reduction of CO_2 under high pressure and high temperature on Pb-granule electrodes in a fixed-bed reactor in aqueous medium. *Applied Catalysis A: General*. 2004; 274(1–2): 237–242.
63. Yano, H., Shirai, F., Nakayama, M. and Ogura, K. Efficient electrochemical conversion of CO_2 to CO, C_2H_4 and CH_4 at a three-phase interface on a Cu net electrode in acidic solution. *Journal of Electroanalytical Chemistry*. 2002; 519(1–2): 93–100.
64. Schizodimou, A. and Kyriacou, G. Acceleration of the reduction of carbon dioxide in the presence of multivalent cations. *Electrochimica Acta*. 2012; 78(0): 171–176.
65. Hori, Y. and Suzuki, S. Electrolytic reduction of carbon dioxide at mercury electrode in aqueous solution. *Bulletin of the Chemical Society of Japan*. 1982; 55(3): 660–665.
66. Studt, F., Sharafutdinov, I., Abild-Pedersen, F., Elkjær, C. F., Hummelshøj, J. S., Dahl, S., Chorkendorff, I. and Nørskov, J. K. Discovery of a Ni-Ga catalyst for carbon dioxide reduction to methanol. *Nature Chemistry*. 2014; 6(4): 320–324.
67. Behrens, M., Studt, F., Kasatkin, I., Kühl, S., Hävecker, M., Abild-Pedersen, F., Zander, S., Girgsdies, F., Kurr, P., Kniep, B.-L., Tovar, M., Fischer, R. W., Nørskov, J. K. and Schlögl, R. The active site of methanol synthesis over $Cu/ZnO/Al_2O_3$ industrial catalysts. *Science*. 2012; 336(6083): 893–897.

68. Herman, R. G., Klier, K., Simmons, G. W., Finn, B. P., Bulko, J. B. and Kobylinski, T. P. Catalytic synthesis of methanol from COH_2: I. Phase composition, electronic properties, and activities of the $Cu/ZnO/M_2O_3$ catalysts. *Journal of Catalysis*. 1979; 56(3): 407–429.
69. Bailey, S., Froment, G. F., Snoeck, J. W. and Waugh, K. C. A DRIFTS study of the morphology and surface adsorbate composition of an operating methanol synthesis catalyst. *Catalysis Letters*. 1995; 30(1–4): 99–111.
70. Sheffer, G. R. and King, T. S. Potassium's promotional effect of unsupported copper catalysts for methanol synthesis. *Journal of Catalysis*. 1989; 115(2): 376–387.
71. Cox, D. F. and Schulz, K. H. Methanol decomposition on single crystal Cu_2O. *Journal of Vacuum Science & Technology A*. 1990; 8(3): 2599–2604.
72. Peterson, A. A., Abild-Pedersen, F., Studt, F., Rossmeisl, J. and Norskov, J. K. How copper catalyzes the electroreduction of carbon dioxide into hydrocarbon fuels. *Energy & Environmental Science*. 2010; 3(9): 1311–1315.
73. Le, M. T. H. *Electrochemical Reduction of CO_2 to Methanol*. Louisiana State University, Louisiana, 2011.
74. Yang, Y., Evans, J., Rodriguez, J. A., White, M. G. and Liu, P. Fundamental studies of methanol synthesis from CO_2 hydrogenation on Cu (111), Cu clusters, and Cu/ZnO (0001 [combining macron]). *Physical Chemistry Chemical Physics*. 2010; 12(33): 9909–9917.
75. Gattrell, M., Gupta, N. and Co, A. A review of the aqueous electrochemical reduction of CO_2 to hydrocarbons at copper. *Journal of Electroanalytical Chemistry*. 2006; 594(1): 1–19.
76. Aylmer-Kelly, A. W. B., Bewick, A., Cantrill, P. R. and Tuxford, A. M. Studies of electrochemically generated reaction intermediates using modulated specular reflectance spectroscopy. *Faraday Discussions of the Chemical Society*. 1973; 56(0): 96–107.
77. Buxton, G. V. and Sellers, R. M. Acid dissociation constant of the carboxyl radical. Pulse radiolysis studies of aqueous solutions of formic acid and sodium formate. *Journal of the Chemical Society, Faraday Transactions 1: Physical Chemistry in Condensed Phases*. 1973; 69(0): 555–559.
78. Bagotzky, V. and Osetrova, N. Electrochemical reduction of carbon dioxide. *Russian Journal of Electrochemistry*. 1995; 31(5): 409–425.
79. Hammouche, M., Lexa, D., Momenteau, M. and Saveant, J. M. Chemical catalysis of electrochemical reactions. Homogeneous catalysis of the electrochemical reduction of carbon dioxide by iron("0") porphyrins. Role of the addition of magnesium cations. *Journal of the American Chemical Society*. 1991; 113(22): 8455–8466.
80. Gressin, J., Michelet, D., Nadjo, L. and Savéant, J. Electrochemical reduction of carbondioxide in low proton media. *Nouveau Journal De Chimie-New Journal of Chemistry*. 1979; 3(8–9): 545–554.
81. Amatore, C. and Saveant, J. M. Mechanism and kinetic characteristics of the electrochemical reduction of carbon dioxide in media of low proton availability. *Journal of the American Chemical Society*. 1981; 103(17): 5021–5023.
82. Gennaro, A., Isse, A. A., Severin, M.-G., Vianello, E., Bhugun, I. and Saveant, J.-M. Mechanism of the electrochemical reduction of carbon dioxide at inert electrodes in media of low proton availability. *Journal of the Chemical Society, Faraday Transactions*. 1996; 92(20): 3963–3968.
83. Beley, M., Collin, J. P., Ruppert, R. and Sauvage, J. P. Electrocatalytic reduction of carbon dioxide by nickel cyclam2+ in water: Study of the factors affecting the efficiency and the selectivity of the process. *Journal of the American Chemical Society*. 1986; 108(24): 7461–7467.
84. Shionoya, M., Kimura, E. and Iitaka, Y. Mono-, di- and tetrafluorinated cyclams. *Journal of the American Chemical Society*. 1990; 112(25): 9237–9245.

85. Benson, E. E., Kubiak, C. P., Sathrum, A. J. and Smieja, J. M. Electrocatalytic and homogeneous approaches to conversion of CO_2 to liquid fuels. *Chemical Society Reviews*. 2009; 38(1): 89–99.
86. Beley, M., Collin, J.-P., Ruppert, R. and Sauvage, J.-P. Nickel(II)-cyclam: An extremely selective electrocatalyst for reduction of CO_2 in water. *Journal of the Chemical Society, Chemical Communications*. 1984; (19): 1315–1316.
87. Costentin, C., Robert, M. and Saveant, J.-M. Catalysis of the electrochemical reduction of carbon dioxide. *Chemical Society Reviews*. 2013; 42(6): 2423–2436.
88. Costentin, C., Drouet, S., Robert, M. and Savéant, J.-M. A local proton source enhances CO_2 electroreduction to CO by a molecular Fe catalyst. *Science*. 2012; 338(6103): 90–94.
89. Rakowski Dubois, M. and Dubois, D. L. Development of molecular electrocatalysts for CO_2 reduction and H2 production/oxidation. *Accounts of Chemical Research*. 2009; 42(12): 1974–1982.
90. DuBois, D. L., Miedaner, A. and Haltiwanger, R. C. Electrochemical reduction of carbon dioxide catalyzed by [Pd(triphosphine)(solvent)](BF4)2 complexes: Synthetic and mechanistic studies. *Journal of the American Chemical Society*. 1991; 113(23): 8753–8764.
91. Raebiger, J. W., Turner, J. W., Noll, B. C., Curtis, C. J., Miedaner, A., Cox, B. and DuBois, D. L. Electrochemical reduction of CO_2 to CO catalyzed by a bimetallic palladium complex. *Organometallics*. 2006; 25(14): 3345–3351.
92. Grice, K. A., Gu, N. X., Sampson, M. D. and Kubiak, C. P. Carbon monoxide release catalysed by electron transfer: Electrochemical and spectroscopic investigations of [Re(bpy-R)(CO)4](OTf) complexes relevant to CO_2 reduction. *Dalton Transactions*. 2013; 42(23): 8498–8503.
93. Smieja, J. M. and Kubiak, C. P. Re(bipy-tBu)(CO)3Cl– improved catalytic activity for reduction of carbon dioxide: IR-spectroelectrochemical and mechanistic studies. *Inorganic Chemistry*. 2010; 49(20): 9283–9289.
94. Benson, E. E., Sampson, M. D., Grice, K. A., Smieja, J. M., Froehlich, J. D., Friebel, D., Keith, J. A., Carter, E. A., Nilsson, A. and Kubiak, C. P. The electronic states of rhenium bipyridyl electrocatalysts for CO_2 reduction as revealed by X-ray absorption spectroscopy and computational quantum chemistry. *Angewandte Chemie International Edition*. 2013; 52(18): 4841–4844.
95. Hawecker, J., Lehn, J.-M. and Ziessel, R. Electrocatalytic reduction of carbon dioxide mediated by Re(bipy)(CO)3Cl (bipy = 2,2[prime or minute]-bipyridine). *Journal of the Chemical Society, Chemical Communications*. 1984; (6): 328–330.
96. Smieja, J. M., Benson, E. E., Kumar, B., Grice, K. A., Seu, C. S., Miller, A. J. M., Mayer, J. M. and Kubiak, C. P. Kinetic and structural studies, origins of selectivity, and interfacial charge transfer in the artificial photosynthesis of CO. *Proceedings of the National Academy of Sciences*. 2012; 109(39): 15646–15650.
97. Ishida, H., Tanaka, K. and Tanaka, T. Electrochemical CO_2 reduction catalyzed by ruthenium complexes [Ru(bpy)2(CO)2]2+ and [Ru(bpy)2(CO)Cl]+. Effect of pH on the formation of CO and HCOO. *Organometallics*. 1987; 6(1): 181–186.
98. Angamuthu, R., Byers, P., Lutz, M., Spek, A. L. and Bouwman, E. Electrocatalytic CO_2 conversion to oxalate by a copper complex. *Science*. 2010; 327(5963): 313–315.
99. Barton Cole, E., Lakkaraju, P. S., Rampulla, D. M., Morris, A. J., Abelev, E. and Bocarsly, A. B. Using a one-electron shuttle for the multielectron reduction of CO_2 to methanol: Kinetic, mechanistic, and structural insights. *Journal of the American Chemical Society*. 2010; 132(33): 11539–11551.
100. Seshadri, G., Lin, C. and Bocarsly, A. B. A new homogeneous electrocatalyst for the reduction of carbon dioxide to methanol at low overpotential. *Journal of Electroanalytical Chemistry*. 1994; 372(1–2): 145–150.

101. Barton, E. E., Rampulla, D. M. and Bocarsly, A. B. Selective solar-driven reduction of CO_2 to methanol using a catalyzed p-GaP based photoelectrochemical cell. *Journal of the American Chemical Society*. 2008; 130(20): 6342–6344.
102. Taniguchi, I., Aurian-Blajeni, B. and Bockris, J. O. M. The mediation of the photoelectrochemical reduction of carbon dioxide by ammonium ions. *Journal of Electroanalytical Chemistry and Interfacial Electrochemistry*. 1984; 161(2): 385–388.
103. Bockris, J. M. and Wass, J. The photoelectrocatalytic reduction of carbon dioxide. *Journal of the Electrochemical Society*. 1989; 136(9): 2521–2528.
104. Kyriacou, G. and Anagnostopoulos, A. Electroreduction of CO_2 on differently prepared copper electrodes: The influence of electrode treatment on the current efficiences. *Journal of Electroanalytical Chemistry*. 1992; 322(1–2): 233–246.
105. DeWulf, D. W., Jin, T. and Bard, A. J. Electrochemical and surface studies of carbon dioxide reduction to methane and ethylene at copper electrodes in aqueous solutions. *Journal of the Electrochemical Society*. 1989; 136(6): 1686–1691.
106. Shiratsuchi, R., Aikoh, Y. and Nogami, G. Pulsed electroreduction of CO copper electrodes. *Journal of the Electrochemical Society*. 1993; 140(12): 3479–3482.
107. Smith, B., Irish, D., Kedzierzawski, P. and Augustynski, J. A surface enhanced Raman scattering study of the intermediate and poisoning species formed during the electrochemical reduction of CO_2 on copper. *Journal of the Electrochemical Society*. 1997; 144(12): 4288–4296.
108. Cook, R. L., MacDuff, R. C. and Sammells, A. F. On the electrochemical reduction of carbon dioxide at in situ electrodeposited copper. *Journal of the Electrochemical Society*. 1988; 135(6): 1320–1326.
109. Friebe, P., Bogdanoff, P., Alonso-Vante, N. and Tributsch, H. A real-time mass spectroscopy study of the (electro)chemical factors affecting CO_2 reduction at copper. *Journal of Catalysis*. 1997; 168(2): 374–385.
110. Grodkowski, J., Dhanasekaran, T., Neta, P., Hambright, P., Brunschwig, B. S., Shinozaki, K. and Fujita, E. Reduction of cobalt and iron phthalocyanines and the role of the reduced species in catalyzed photoreduction of CO2. *The Journal of Physical Chemistry A*. 2000; 104(48): 11332–11339.
111. Kuhl, K. P., Cave, E. R., Abram, D. N. and Jaramillo, T. F. New insights into the electrochemical reduction of carbon dioxide on metallic copper surfaces. *Energy & Environmental Science*. 2012; 5(5): 7050–7059.
112. Peterson, A. A. and Nørskov, J. K. Activity descriptors for CO_2 electroreduction to methane on transition-metal catalysts. *The Journal of Physical Chemistry Letters*. 2012; 3(2): 251–258.
113. Durand, W. J., Peterson, A. A., Studt, F., Abild-Pedersen, F. and Nørskov, J. K. Structure effects on the energetics of the electrochemical reduction of CO_2 by copper surfaces. *Surface Science*. 2011; 605(15–16): 1354–1359.
114. Frese, K. W. Electrochemical reduction of CO_2 at intentionally oxidized copper electrodes. *Journal of the Electrochemical Society*. 1991; 138(11): 3338–3344.
115. Le, M., Ren, M., Zhang, Z., Sprunger, P. T., Kurtz, R. L. and Flake, J. C. Electrochemical reduction of CO_2 to CH_3OH at copper oxide surfaces. *Journal of the Electrochemical Society*. 2011; 158(5): E45–E49.
116. Cook, R. L., Macdugg, R. and Sammells, A. F. Gas-phase CO_2 reduction to hydrocarbons at metal/solid polymer electrolyte interface. *Journal of the Electrochemical Society*. 1990; 137(1): 187–189.
117. Whipple, D. T., Finke, E. C. and Kenis, P. J. Microfluidic reactor for the electrochemical reduction of carbon dioxide: The effect of pH. *Electrochemical and Solid-State Letters*. 2010; 13(9): B109–B111.
118. Spinner, N. S., Vega, J. A. and Mustain, W. E. Recent progress in the electrochemical conversion and utilization of CO_2. *Catalysis Science & Technology*. 2012; 2(1): 19–28.

119. Innocent, B., Liaigre, D., Pasquier, D., Ropital, F., Léger, J. M. and Kokoh, K. B. Electro-reduction of carbon dioxide to formate on lead electrode in aqueous medium. *Journal of Applied Electrochemistry*. 2009; 39(2): 227–232.
120. Azuma, M., Hashimoto, K., Hiramoto, M., Watanabe, M. and Sakata, T. Electrochemical reduction of carbon dioxide on various metal electrodes in low-temperature aqueous $KHCO_3$ media. *Journal of the Electrochemical Society*. 1990; 137(6): 1772–1778.
121. Köleli, F., Atilan, T., Palamut, N., Gizir, A. M., Aydin, R. and Hamann, C. H. Electrochemical reduction of CO_2 at Pb- and Sn-electrodes in a fixed-bed reactor in aqueous K_2CO_3 and $KHCO_3$ media. *Journal of Applied Electrochemistry*. 2003; 33(5): 447–450.
122. Hara, K., Kudo, A. and Sakata, T. Electrochemical reduction of carbon dioxide under high pressure on various electrodes in an aqueous electrolyte. *Journal of Electroanalytical Chemistry*. 1995; 391(1–2): 141–147.
123. Popić, J. P., Avramov-Ivić, M. L. and Vuković, N. B. Reduction of carbon dioxide on ruthenium oxide and modified ruthenium oxide electrodes in 0.5 M $NaHCO_3$. *Journal of Electroanalytical Chemistry*. 1997; 421(1–2): 105–110.
124. Frese, K. and Leach, S. Electrochemical reduction of carbon dioxide to methane, methanol, and CO on Ru electrodes. *Journal of the Electrochemical Society*. 1985; 132(1): 259–260.
125. Furuya, N., Yamazaki, T. and Shibata, M. High performance Ru Society of carbon dioxide to methane, metiffusion electrodes. *Journal of Electroanalytical Chemistry*. 1997; 431(1): 39–41.
126. Hoshi, N., Suzuki, T. and Hori, Y. Step density dependence of CO_2 reduction rate on Pt(S)-[n(111) × (111)] single crystal electrodes. *Electrochimica Acta*. 1996; 41(10): 1647–1653.
127. Hoshi, N., Suzuki, T. and Hori, Y. CO_2 reduction on Pt(S) – [n(111) × (111)] single crystal electrodes affected by the adsorption of sulfuric acid anion. *Journal of Electroanalytical Chemistry*. 1996; 416(1–2): 61–65.
128. Hara, K., Tsuneto, A., Kudo, A. and Sakata, T. Electrochemical reduction of CO_2 on a Cu electrode under high pressure factors that determine the product selectivity. *Journal of the Electrochemical Society*. 1994; 141(8): 2097–2103.
129. Kaneco, S., Hiei, N.-h., Xing, Y., Katsumata, H., Ohnishi, H., Suzuki, T. and Ohta, K. Electrochemical conversion of carbon dioxide to methane in aqueous $NaHCO_3$ solution at less than 273 K. *Electrochimica Acta*. 2002; 48(1): 51–55.
130. Kaneco, S., Katsumata, H., Suzuki, T., Ohta, K., Liu, C.-j., Mallinson, R. G. and Aresta, M. *Utilization of Greenhouse Gases: Electrochemical Reduction of CO2 on Cu Electrode in Methanol at Low Temperature*. American Chemical Society, Washington, DC, 2003.
131. Rosen, B. A., Haan, J. L., Mukherjee, P., Braunschweig, B., Zhu, W., Salehi-Khojin, A., Dlott, D. D. and Masel, R. I. In situ spectroscopic examination of a low overpotential pathway for carbon dioxide conversion to carbon monoxide. *The Journal of Physical Chemistry C*. 2012; 116(29): 15307–15312.
132. Asadi, M., Kumar, B., Behranginia, A., Rosen, B. A., Baskin, A., Repnin, N., Pisasale, D., Phillips, P., Zhu, W., Haasch, R., Klie, R. F., Kral, P., Abiade, J. and Salehi-Khojin, A. Robust carbon dioxide reduction on molybdenum disulphide edges. *Nature Communications*. 2014; 5: 4470.
133. Rosen, B. A., Zhu, W., Kaul, G., Salehi-Khojin, A. and Masel, R. I. Water enhancement of CO_2 conversion on silver in 1-ethyl-3-methylimidazolium tetrafluoroborate. *Journal of the Electrochemical Society*. 2013; 160(2): H138–H141.
134. Łukaszewski, M., Siwek, H. and Czerwiński, A. Electrosorption of carbon dioxide on platinum group metals and alloys—A review. *Journal of Solid State Electrochemistry*. 2009; 13(6): 813–827.

135. Whipple, D. T. and Kenis, P. J. A. Prospects of CO_2 utilization via direct heterogeneous electrochemical reduction. *The Journal of Physical Chemistry Letters*. 2010; 1(24): 3451–3458.
136. Chandrasekaran, K. and Bockris, L. O. M. In-situ spectroscopic investigation of adsorbed intermediate radicals in electrochemical reactions: CO_2^- on platinum. *Surface Science*. 1987; 185(3): 495–514.